Pergamon

Geochimica et Cosmochimica Acta, Vol. 64, No. 23, pp. 4049–4081, 2000

0016-7037/00 $20.00 + .00

PII S0016-7037(00)00481-6

Elongated prismatic magnetite crystals in ALH84001 carbonate globules: Potential Martian magnetofossils

KATHIE L. THOMAS-KEPRTA,[1,*] DENNIS A. BAZYLINSKI,[2] JOSEPH L. KIRSCHVINK,[3] SIMON J. CLEMETT,[1] DAVID S. MCKAY,[4] SUSAN J. WENTWORTH,[1] HOJATOLLAH VALI[5], EVERETT K. GIBSON JR.[6], and CHRISTOPHER S. ROMANEK[7]

[1]Lockheed Martin, 2400 NASA Rd. 1, Mail Code C23, Houston, TX 77058, USA
[2]Iowa State University, Dept. of Microbiology, 207 Science I, Ames, IA 50011, USA
[3]California Institute of Technology, Div. of Geological and Planetary Sciences, 1200 E. California Blvd., Pasadena, CA 91125, USA
[4]NASA/Johnson Space Center, Mail Code SN, Houston, TX 77058, USA
[5]McGill University, Dept. of Earth and Planetary Sciences, 3450 University St., Montreal, PQ H3A 2A7, Canada
[6]NASA/Johnson Space Center, Mail Code SN2, Houston, TX 77058, USA
[7]Savannah River Ecology Laboratory, Drawer E, University of Georgia, Aiken, SC 29802, USA

(*Received December* 7, 1999; *accepted in revised form May* 30, 2000)

Abstract—Using transmission electron microscopy (TEM), we have analyzed magnetite (Fe_3O_4) crystals acid-extracted from carbonate globules in Martian meteorite ALH84001. We studied 594 magnetites from ALH84001 and grouped them into three populations on the basis of morphology: 389 were irregularly shaped, 164 were elongated prisms, and 41 were whisker-like.

As a possible terrestrial analog for the ALH84001 elongated prisms, we compared these magnetites with those produced by the terrestrial magnetotactic bacteria strain MV-1. By TEM again, we examined 206 magnetites recovered from strain MV-1 cells. Natural (Darwinian) selection in terrestrial magnetotactic bacteria appears to have resulted in the formation of intracellular magnetite crystals having the physical and chemical properties that optimize their magnetic moment. In this study, we describe six properties of magnetite produced by biologically controlled mechanisms (e.g., magnetotactic bacteria), properties that, collectively, are not observed in any known population of inorganic magnetites.

These criteria can be used to distinguish one of the modes of origin for magnetites from samples with complex or unknown histories. Of the ALH84001 magnetites that we have examined, the elongated prismatic magnetite particles (~27% of the total) are indistinguishable from the MV-1 magnetites in five of these six characteristics observed for biogenically controlled mineralization of magnetite crystals. *Copyright © 2000 Elsevier Science Ltd*

1. INTRODUCTION

The first meteorite processed in 1984 from the Allan Hills area of Antarctica, therefore dubbed "ALH84001," was recognized in 1994 as one of a group of just over a dozen meteorites whose isotopic chemistry, including atmospheric gases trapped in some of them, shows that they came to Earth from Mars. In 1996, D. S. McKay et al., presented four lines of evidence leading them to believe that this Martian meteorite contained signs of fossil life. In this paper we describe further work to support one of these lines of evidence—that fine-grained magnetite (Fe_3O_4) crystals located within the Fe-rich rims of the carbonate globules in ALH84001 resemble magnetites produced by magnetotactic bacteria.

To distinguish magnetite produced by biologically controlled processes from magnetite produced by other mechanisms, we establish a set of six criteria. These criteria include specific physical and chemical characteristics that, when considered collectively, are not observed in any known population of inorganic magnetites. We use these criteria to evaluate the origins of magnetites extracted from ALH84001 carbonate globules.

The crystallographic age of ALH84001, ~4.5 Ga (Nyquist et al., 1995), makes it the oldest of the Martian meteorites so far found on Earth. The carbonate globules within ALH84001 have been dated as ~3.9 Ga old (Borg et al., 1999). Textural and isotopic evidence shows that these carbonate globules were formed on Mars (Romanek et al., 1994; McKay et al., 1996; Treiman, 1998). Microtomed thin sections of carbonate globules show that magnetites are embedded within the carbonate matrix. If the carbonate globules are Martian, then by association the magnetites are also of Martian origin. Furthermore, these magnetites have experienced little oxidation during their 13,000 year residence time (Jull et al., 1995) on Earth. We have not observed the oxidation of nanometer-sized magnetites in ALH84001 to maghemite (γ-Fe_2O_3) or hematite (α-Fe_2O_3). Nanometer-size magnetite is rapidly oxidized to these phases in aqueous solutions below pH 8 (Nicholls, 1987). Since the near-surface environment on the ice fields of Antarctica is oxidizing (nearly all Antarctic meteorites show evidence for rust on their outer surfaces (Gooding, 1992)), the lack of maghemite and hematite suggests that the magnetites in ALH84001 are pristine. The ALH84001 magnetites had to have been protected from oxidation by being encased in the carbonate matrix during their residence in Antarctica.

Magnetite crystals in ALH84001 generally range from ~10 to 100 nm in size and have cuboid, teardrop, or irregular shapes (McKay et al., 1996). Magnetite crystals with these shapes are found throughout the ALH84001 carbonate globules in both the rims (Thomas-Keprta et al., 1998; 1999) and the interiors (Bradley et al., 1996; Thomas-Keprta et al., 1998), although

*Author to whom correspondence should be addressed (kthomas@ems.jsc.nasa.gov).

they are most concentrated in the optically dark rims. Crystals with fiber- or needle-shaped projections have only been reported in the globule interiors (Bradley et al., 1996).

Magnetite in terrestrial samples can be produced either abiotically or biogenically. The biomineralization of magnetite by bacteria occurs by two fundamentally different modes: (1) biologically controlled (Lowenstam, 1981; Mann, 1986) and (2) biologically induced (Lowenstam, 1981; Mann, 1986). In biologically controlled mineralization, magnetotactic bacteria produce well-ordered intracellular crystals of magnetite that exhibit narrow size distributions and consistent species- and/or strain-specific morphologies (Towe and Moench, 1981; Mann et al., 1984b; Mann and Frankel, 1989; Stolz et al., 1990; Sparks et al., 1990; Meldrum et al., 1993b; Bazylinski, 1995; Bazylinski and Moskowitz, 1997). Magnetotactic bacteria appear to exert strict genetic control over the composition, size, morphology, and crystallographic orientation of their internal magnetite particles by precipitating them within small intracellular membrane vesicles; this assemblage is known as a magnetosome. It is currently thought that components of this magnetosome may control the biomineralization processes in magnetite synthesis (Gorby et al., 1988).

Magnetotactic bacteria exploit the magnetic moment generated by their intracellular magnetite crystals by passively aligning along the Earth's geomagnetic field lines like a compass needle (Blakemore, 1975; Frankel et al., 1979). Together with aerotaxis and other forms of chemotaxis and/or redoxtaxis, magnetotaxis allows cells to more efficiently locate and maintain an optimal position in vertical chemical and/or redox gradients (e.g., dissolved oxygen) by reducing a three-dimensional search problem to a one-dimensional one (Kirschvink,1980; Frankel et al., 1997).

At least six specific properties, described below in detail, increase the efficiency of magnetization and have likely evolved through the process of natural (Darwinian) selection. We suggest that, when considered collectively, these criteria constitute a biosignature. Some of these criteria have been used informally for nearly 20 years to identify the fossil remnants of bacterial magnetosomes (magnetofossils) in the sedimentary rock record on Earth (e.g., Chang et al., 1987; McNeill et al, 1988; Chang and Kirschvink, 1989; Hesse, 1994; Schwartz et al., 1997). However, this is the first time that all six criteria have been described and interpreted collectively as a biosignature that can be applied to any terrestrial and extraterrestrial samples containing magnetite. Each of these six criteria is discussed in detail below.

1.1. Single-Domain Size and Restricted Anisotropic Width/Length Ratios

The physical volume and shape of individual magnetite crystals determine how well grains function as discrete bar magnets. As magnetite is ferrimagnetic below 580°C, all crystals will have a spontaneous and permanent magnetic moment at room temperature. However, thermal fluctuations will cause the magnetic moment to wander relative to the crystallographic axes when the grains are below a certain size, where particles exhibit superparamagnetic behavior (i.e., do not hold a stable net magnetization). As crystal size increases, the energy stored in the magnetic field surrounding the crystal becomes larger than the energy needed to nucleate magnetic domain-wall boundaries, and the magnetic moment of the particle collapses into a series of self-canceling vectors, yielding a multi-domain state. Between these two extremes is a region of single-domain behavior, where the particle is uniformly magnetized and the magnetic moment is locked to the crystal lattice. Particles within this size and shape range are perfect bar magnets.

All tests of the magnetosome crystals from living magnetotactic bacteria, done by comparing the physical size and shape requirements for single-domain behavior (Butler and Banerjee, 1975; Diaz-Ricci and Kirschvink, 1992) with the measured size and shape of the magnetosome crystals, have confirmed this relationship (Kirschvink and Lowenstam, 1979; Towe and Moench, 1981; Kirschvink, 1983; Mann et al., 1984a; b; Mann, 1985; Mann et al., 1987b; Mann et al., 1987a; Mann and Frankel, 1989; Stolz et al., 1990; Mann et al., 1991; Meldrum et al., 1993b; Bazylinski, 1995; Bazylinski and Moskowitz, 1997; Sparks et al., 1990; this work). This relationship arises from natural selection, as superparamagnetic or multi-domain crystals are of no value for magnetotaxis (Kirschvink and Lowenstam, 1979), so biogenic crystals display restricted width/length (W/L) ratios and volumes within the single-domain size range for a competitive advantage in the natural environment (e.g., magnetotactic bacteria strain MV-1).

1.2. Chemical Purity

Magnetite produced by magnetotactic bacteria is generally pure stoichiometric Fe_3O_4, lacking minor or significant trace elements such as Ti, Cr, Mn, and Al (e.g., Lowenstam, 1981; Mann, 1986; Bazylinski and Moskowitz, 1997; Mann and Frankel, 1989; Bazylinski, 1995; Stolz et al., 1990; Meldrum et al., 1993a; b; Towe and Moench, 1981; Sparks et al., 1990; this work) with few exceptions (Towe and Moench, 1981). Magnetotactic bacteria exclude these other elements from the growing magnetite crystals, even though the elements may be readily available in the environment (Gorby, 1989; this work). Such high chemical specificity is typical of bacterial pathways for Fe acquisition and transport, which involve multiple chelation and redox steps linked with ATP-coupled transport across lipid-bilayer membranes (Braun et al., 1998). Some magnetotactic bacteria such as *Magnetospirillum magnetotacticum* are thought to produce highly Fe-selective siderophores (Paoletti and Blakemore, 1986) to accumulate Fe within their magnetosome membrane vesicles (Gorby et al., 1988). Since Ti, Al, and most other chemical impurities reduce the saturation magnetization of magnetite, it is possible that this selectivity is a product of natural selection.

1.3. Crystallographic Perfection

High-resolution transmission electron microscope studies of the magnetite crystals formed by magnetotactic bacteria indicate they are essentially free of internal defects, with the minor exception of an occasional twin in the {111} plane (Vali et al., 1987; Vali and Kirschvink, 1991; Mann et al., 1988; Devouard et al., 1998). The lack of lattice defects acts to increase the net magnetic moment of the particle. Consequently, the ability to grow defect-free crystals may be a product of natural selection. As the [111] direction is the magnetically "easy" axis in mag-

netite, twins across this plane have no effect on their magnetization efficiency.

1.4. Magnetite Chains

Virtually all magnetotactic organisms arrange their magnetite crystals in linear chains. The total magnetic moment of the cell is the vector sum of the moments of each of the individual crystals, arranged linearly, which serves to maximize the total magnetic moment of the cell. For example, a typical magnetosome from bacterial strain MV-1 (Bazylinski and Moskowitz, 1997; Sparks et al., 1990), has a magnetic to thermal orientation energy ratio (μB/kT) of about 0.5, implying that Brownian motion easily disrupts its alignment in the geomagnetic field. Aligning 20 such crystals in the chain will bring this energy ratio up to $\sim$10, providing the bacterium with very good passive alignment (Frankel and Blakemore, 1980). However, this linear arrangement is dynamically unstable (Kirschvink, 1982), and therefore crystal chains have a strong tendency to rotate and collapse, reducing the energy of the magnetic field of a cell. The magnetostatic potential energy difference between a typical straight bacterial magnetosome chain and that of a clump of crystals is on the order of 10^3 kT (Kirschvink, 1982). As bacteria lack a dynamic cytoskeletal system which could overcome this energy barrier, they must form chains by synthesizing them de novo, creating new magnetosomes directly at the end of an existing chain and anchoring them (i.e., not free-floating, individual magnetite crystals in cytoplasm) (Gorby et al., 1988). When the organism dies, the magnetosome membrane decomposes and the magnetostatic potential energy dissipates by collapsing upon itself. Biogenic magnetites found embedded in recent terrestrial samples and as fossil remains in ancient samples often show no evidence for chains (e.g., Chang et al., 1989; Chang and Kirschvink, 1989).

1.5. Unusual Crystal Morphology

Some magnetite crystal shapes produced by some magnetotactic bacteria are anisotropic (e.g., bullet-shaped, elongated hexagonal prismatic particles) and are not typical of those formed inorganically (e.g., Mann et al., 1991). For inorganic particles smaller than a micrometer, a significant fraction of their total energy exists as surface free energy. Because the driving force behind crystal growth is the minimization of surface free energy, minerals of the isometric crystal system such as magnetite adopt isotropic forms (e.g., cubic, cubo-octahedral, octahedral, dodecahedral) (Ichinose et al., 1992). For larger crystals ($>$10 μm), anisotropic crystal shapes commonly occur due to heterogeneous growth in microenvironments characterized by local concentration gradients (Nicholls, 1987; Symonds, 1993).

Understanding crystal growth is important in interpreting the unusual elongated hexagonal morphology of magnetites produced by bacterial strain MV-1 (Bazylinski and Moskowitz, 1997; Sparks et al., 1990), which is not the thermodynamic equilibrium shape that would be expected for particles of this size, for reasons discussed above. These crystals are composed of 14 faces; eight equivalent {111} faces separated by six {110} equivalent faces elongated along one of the [111] axes, forming a hexagonal prism with faceted ends (Mann et al., 1991). In projection under the electron microscope beam, elongated magnetite particles, such as those of strain MV-1, appear rectangular and have therefore been described as "parallelepipeds" (e.g., Bazylinski et al., 1988) which, in a technical crystallographic sense, is incorrect. Although never explicitly mentioned in the literature, the name "hexaoctahedron" has been suggested to us (George W. Hart, private communication), emphasizing that it has six {110} hexagonal faces and eight {111} octahedral faces.

In a crystal with hexaoctahedral geometry, growth along all [111] axes should be equivalent. The anisotropic morphology of MV-1 magnetite, characterized by preferred growth in one [111] direction [see (vi) below], has been ascribed to genetic control (e.g., the influence of the magnetosome membrane) (Meldrum et al., 1993a; Gorby, 1989). It is possible that the magnetosome membrane physically restricts growth along certain axes by blocking diffusional access to crystal faces once they grow into contact with it. Several other examples of unusual crystal morphology are known for other strains of magnetotactic bacteria (Mann et al., 1991).

Biological elongation permits particles to achieve larger volumes, and hence larger magnetic dipole moments, without crossing into the multi-domain state [see property (i)]. This allows the cells to make fewer magnetosomes to achieve the same magnetic orientation energy. Elongation minimizes the magnetostatic energy associated with the shape anisotropy and forces the moment to lie along the long axis of the crystal, releasing an energy of about 500 kT ($\sim 2 \times 10^{-18}$ J) for the typical MV-1 crystal ($63 \times 37 \times 37$ nm).

1.6. Crystallographic Direction of Elongation of Magnetite Crystals

Another characteristic of magnetite crystals in bacterial magnetosomes is the tendency for the crystals to be elongated along the chain length in one of the [111] directions (Mann et al., 1984a; 1985; 1987b; 1987a; 1988; Vali et al., 1987; Vali and Kirschvink, 1991). For a typical MV-1 magnetosome, alignment of the magnetic moment along the [111] crystallographic direction, rather than the [100] direction, reduces the magnetostatic potential energy by about 4.5 mJ/cm^3, equivalent to about 90 kT for the MV-1 crystals. Two hypotheses have been proposed for this crystallographic alignment (Kirschvink, 1992):

1. The first hypothesis is based on a magnetostatic argument. In some organisms, new magnetosomes are clearly formed at the ends of existing magnetosome chains where both the field and field gradients are intense. Under these conditions, the {111} magnetocrystalline anisotropy energy for an equant superparamagnetic crystal only $\sim$10 nm in size is enough to cause passive alignment with the ambient field direction (Kirschvink, 1992). Continued growth of the crystal within the confines of the magnetosome membrane will then yield [111] elongated particles. This process would not, however, explain the alignment of newly formed magnetosomes in a cell which contains no magnetosomes, a condition that sometimes occurs during cell division. Although this condition is relatively rare, crystals subsequently formed would show the [111] orientation effect.

2. The second hypothesis is based on a genetic control argument. The presence of specific mineral-binding proteins produced by the cell may control the epitaxial nucleation and subsequent growth of the magnetite crystals within the magnetosome membranes.

2. SIX CRITERIA OF A BIOSIGNATURE: SUMMARY

The six criteria described above collectively comprise a biosignature. All six criteria are not always preserved in terrestrial biogenic magnetite, even in the in situ magnetosomes within living bacteria, and some features may be produced through inorganic processes. Confidence with which a potential biological origin is assigned grows with the number of attributes that are expressed. While the database for submicrometer-sized inorganic magnetite crystals is limited, no known population of inorganic magnetite crystals, produced either naturally or synthetically, has met one or two criteria without violating the remaining criteria. A subset of these criteria has been used for nearly 20 years to identify magnetofossils as the carriers of the natural remanent magnetization in a variety of terrestrial sediments (Kirschvink and Lowenstam, 1979; Petersen et al., 1986; Chang et al., 1989; Vali et al., 1989; Vali and Kirschvink, 1989). We propose that the same biological and physical principles may be applicable to fine-grained magnetites from extraterrestrial samples such as those from Mars or any other object in the Solar System. We use these criteria to evaluate the McKay et al. (1996) hypothesis that a subset of the Martian ALH84001 magnetites is of biological origin.

3. METHODS

Two ALH84001 chips containing abundant carbonate globules, identified with optical microscopy, were immersed in ~20 μl of 20% acetic acid (CH_3CO_2H) at 50°C for 72 and 96 hours. Our studies on control samples and dissolution studies by others (Hounslow and Maher, 1996) have shown that this treatment dissolves carbonates of the composition of the globules but has no detectable effect on magnetite. After the chips were removed from the acid, examination by optical microscopy revealed that the carbonate globules were missing. The remaining acid containing the magnetite crystals was placed on carbon-coated TEM copper grids and was allowed to evaporate on a clean bench (Fig. 1). These grids were examined at 160 and 200 kV using a JEOL 2000 FX TEM equipped with a Link System IV energy dispersive x-ray spectrometer (EDS).

Individual magnetite crystals with a range of morphologies were analyzed using EDS with a spot size of ~100 nm for extended times ranging from 500 to 12,000 sec. to determine minor and trace element concentrations. We analyzed individual extracted ALH84001 magnetites in ~50 randomly chosen areas of different TEM grids. These particles were sufficiently isolated so that compositions could be determined for individual grains. We also analyzed some magnetite grains in situ in ultramicrotomed thin sections of ALH84001 carbonate globules. In addition, we analyzed the enclosing carbonate matrix in these sections.

As a control, a microtome thin section (~100 nm thick) of a glass standard [#610 from the National Institute of Standards and Testing (NIST)] was also analyzed. We determined that our limit of detection for Fe was ~150 parts per million (ppm) at 5000 sec.[1]

Magnetite grains within cells of the marine magnetotactic bacterium, strain MV-1 (Bazylinski et al., 1988), were also examined and analyzed. Cells of strain MV-1 were grown anaerobically with nitrous oxide as the terminal electron acceptor under heterotrophic conditions as previously described (Dean and Bazylinski, 1999). Cells were cultured in a growth medium that included a mineral solution containing Ca, Cu, Co, Zn, Mo, Ni, Mg, Al, and Mn (Frankel et al., 1997); some of these elements are required for growth (D. A. Bazylinski, unpublished results). We prepared samples of strain MV-1 magnetites by placing a drop of a MV-1 cell suspension onto a TEM grid and allowing the drop to dry.

MV-1 magnetite particles were chemically analyzed using a JEOL 6340 field emission gun scanning electron microscope (FEGSEM) equipped with an IXRF light element EDS. For this analysis, a drop of the MV-1 cell suspension was placed on a clean brass surface, etched with atomic oxygen to remove cellular material, and rinsed three times in triple-distilled water to remove organic and inorganic debris associated with the cells.

For all types of samples, we determined magnetite crystal dimensions using the TEM at different tilt angles within the limits of our stage (±45°). Magnetite shape and size parameters were obtained from scanned images and their dimensions were estimated by determining the best fit of an oval projection to the irregular particle. The length and width of the projected view of a crystal were matched to the major and minor axes of the best fitting oval. We define these axes as the length and width of the crystal. This technique was determined to have negligible effects on size distributions (Devouard et al., 1998). Modeling studies and the deconvolution of the length and width of magnetite crystals were performed and are discussed below (see Results: Statistical Analyses).

4. RESULTS

4.1. Morphology

Magnetite particles extracted from ALH84001 were found in aggregates consisting of thousands of grains on TEM grids (Fig. 1a). Selected area electron diffraction ring patterns were consistent with that of magnetite (Fig. 1b). Magnetite shapes included cuboidal-, rectangular-, teardrop-, irregular-, platy hexagonal-, and whisker- or rod-shaped morphologies (Fig. 1c). We examined 594 magnetite crystals in ALH84001 and identified three distinct populations: elongated prisms, whisker-shaped, and irregularly shaped (Table A1). We emphasize that this classification is based on morphology, not on size. However, while considerable overlap exists, each magnetite type also has a distinctive size range. We also examined 206 magnetites from magnetotactic bacteria strain MV-1 and found that these crystals were elongated prisms (Table A1). Length, width, and W/L ratio data for ALH84001 magnetites are tabulated in Table A1, which also includes measurements of magnetite crystals from the magnetotactic bacterium strain MV-1. Additional crystal measurements from the magnetotactic bacterial strains MV-1, MV-2, and MC-1, along with extracellular biogenic, commercially produced, and inorganically precipitated magnetite are shown for comparison.

4.1.1. Elongated Prismatic Magnetites

Elongated prismatic magnetites comprised ~27% of the total population. The morphological features of these particles were

[1] The minimum detection limit for Fe was determined using the statistical argument of Joy et al. (1986) that to be *significant* (i.e., detectable) the total signal counts from the Fe-K line, $I_{Fe\text{-}K_\alpha}$, must exceed the total number of counts from the background continuum at the Fe-K line, $I^{Fe\text{–}K_\alpha}_{Continuum}$ by at least $3 \cdot 2 \cdot \sqrt{I^{Fe\text{–}K_\alpha}_{Continuum}}$, where $I^{Fe\text{–}K_\alpha}_{Continuum}$ was determined from the average of the total background continuum just prior to and just after the Fe-K line, that is $I^{Fe\text{–}K_\alpha}_{Continuum} \approx \frac{1}{2} \cdot (I^{Pre(Fe\text{–}K_\alpha)}_{Continuum}) + I^{Post(Fe\text{–}K_\alpha)}_{Continuum})$. Using the NIST Glass Standard #610, we calculated the minimum detection limit for total counts times of 2000 (~200 ppm) and 8000 (~100 ppm) sec. and interpolated the detection sensitivity for Fe of 150 ppm at a count time of 5000 sec.

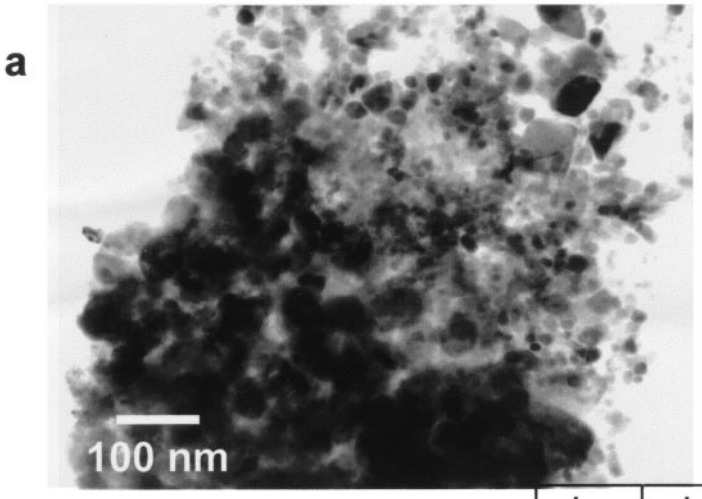

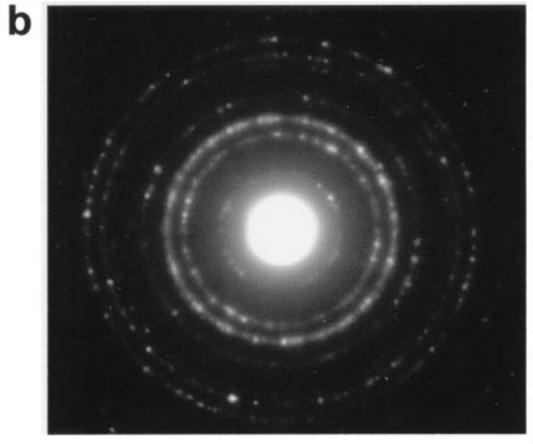

d_{obs} (nm)	d_{exp} (nm)	hkl
0.48	0.4848	111
0.29	0.2969	220
0.25	0.2532	311
0.21	0.2099	400
0.17	0.1713	422
0.16	0.1616	333 or 511
0.15	0.1484	440

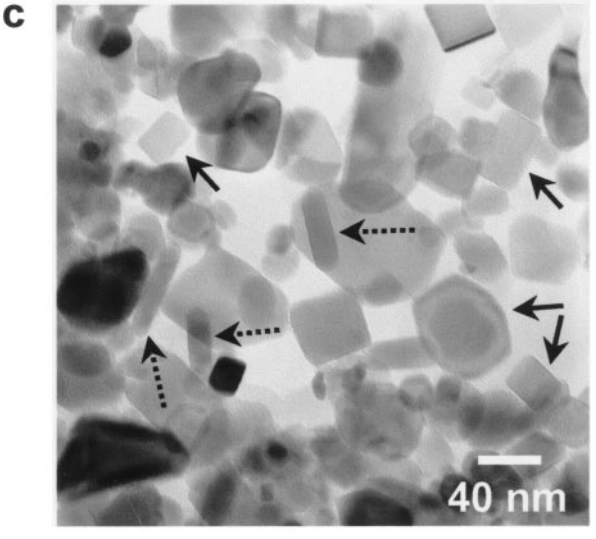

Fig. 1. (a) An aggregate of several hundred magnetite crystals on a TEM grid. These crystals were extracted from the ALH84001 carbonate globules by acid dissolution of the carbonate. (b) Magnetite was identified based on selected area diffraction patterns recorded (experimental data from JCPDS card #19-629). We cannot rule out a small contribution from maghemite or hematite as a result of oxidation of magnetite during the acid dissolution procedure; however, the contribution is too small to be detected. (c) Magnetite morphologies include: irregular, cuboidal, tear-drop, rounded whiskers (dashed arrows), and elongated prisms (solid arrows) which have hexagonal or rectangular projections depending on the angle of stage rotation.

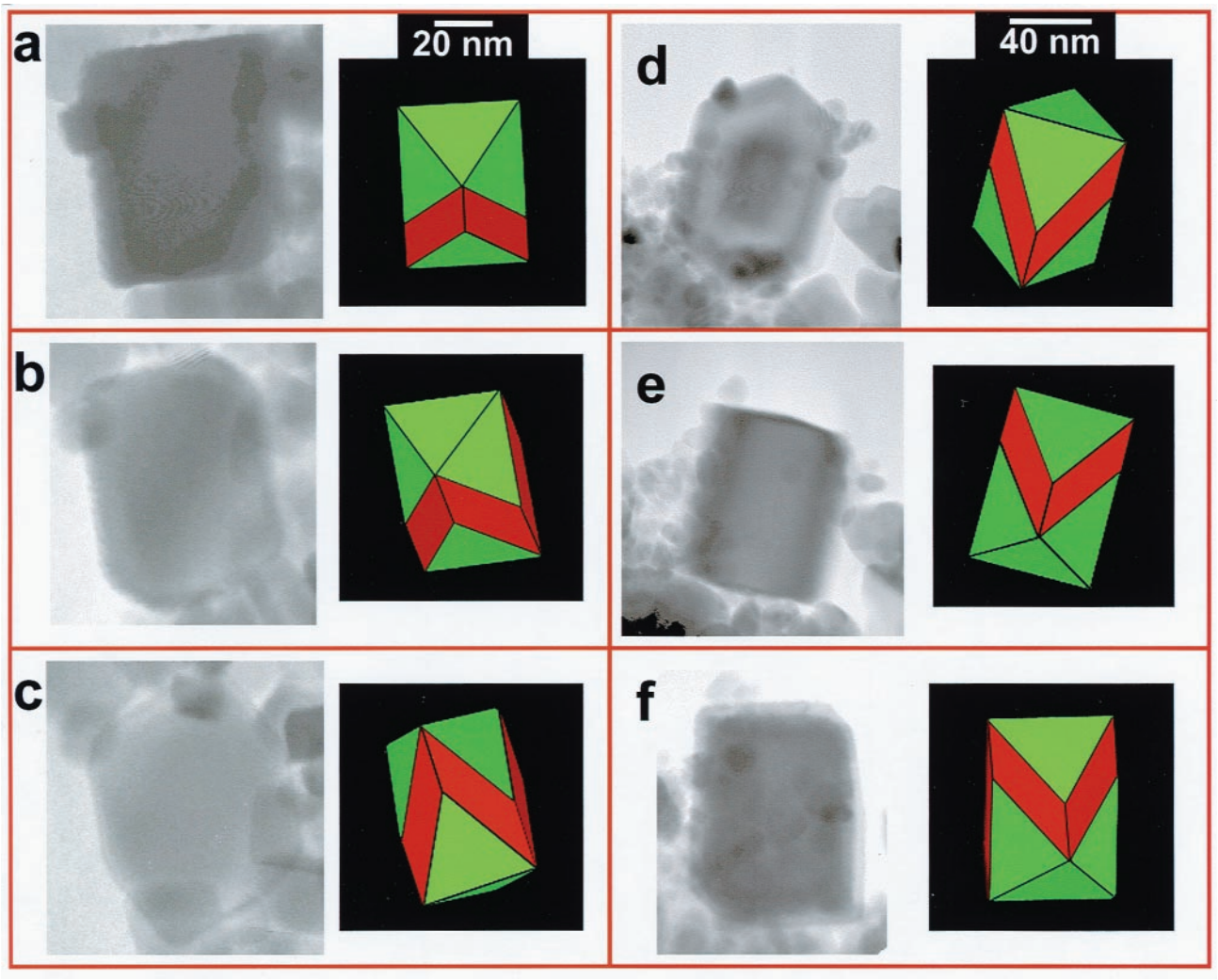

Fig. 2. Six views of two Martian elongated prismatic magnetites: (a) An elongated prismatic magnetite from ALH84001 displaying a rectangular projection at +29°. The same crystal at +6° displaying a rectangular projection with faceted ends on the upper right and lower left corners. (c) The same crystal with a pseudohexagonal projection at −22°. (d–f) An elongated prismatic magnetite displaying a hexagonal cross section at +30° (c) and a rectangular outlines at −10° (d) and −20° (e). Note the faceted edges on the upper right and lower left corners of (f). These faceted edges on crystals shown in (b) and (f) determine the crystal geometry of ALH84001 elongated prismatic particles and are discussed completely in the text. The green models are the two-dimensional projections of the crystals shown in (a–f). Crystals in (a–c) and (d–f) were tilted to a total of ~50° in order to image these particles without interference from underlying and adjacent magnetite grains. If these grains could have been tilted to a total of 90°, then the hexagonal and rectangular views would be closer to perfect (see Figs. 3c–e). However, the magnetite grains were randomly placed on the TEM grid without controlling how the individual crystals lie with respect to each other or the substrate. Magnetite particles from magnetotactic bacteria strain MV-1 were also tilted to similar angles and exhibit both hexagonal and rectangular views (Fig. 6) and projections with faceted edges on opposing corners (Figs. 3q–r).

determined by tilting each of the crystals in the TEM (±45°) to determine the overall shape using multiple projections (Figs. 2 and 3). They are characterized by having hexagonal cross sections (Figs. 2c,d; 3c,d) when viewed along the elongation axis (111 direction) and rectangular cross sections when viewed along the other two perpendicular axes (Figs. 2a,e; 3e-i). Furthermore, these crystals also displayed faceted ends on opposing corners of the rectangular projections in approximately half the observations (Figs. 2b,f). These crystals were anisotropic, always being elongated along the [111] growth direction (Figs. 3a,b) with W/L ratios between 0.4 and 0.9 (a few particles had W/L $>$ 0.9 but none had W/L ratios $<$ 0.4). The mean size of magnetites in this category was ~39 × 27 nm (Table A1).

4.1.2. Whisker Magnetites

These crystals are elongated along one axis and have W/L ratios ranging from ~0.1 to 0.3 (mean 0.2; Table A1). This morphology comprised ~7% of the total population (Figs. 1c and 4). Those with the higher W/L ratios appeared to be whisker shaped when viewed from one direction, but platy

when viewed from a different tilt angle (Fig. 4), while grains having lower W/L ratios displayed both rounded ends and cross sections (see Fig. 1c). None of these whiskers had rectangular or hexagonal projections at any tilt angles. Whisker magnetites with W/L ratios from ~0.1 to 0.2 have been previously reported by Bradley et al. (1996). The mean size of the magnetites in this category was ~76 nm × 11 nm (Table A1).

4.1.3. Irregularly Shaped Magnetites

This category includes crystals with shapes (e.g., cuboidal, teardrop; Fig. 1) not obviously belonging to either the whisker or the elongated prismatic group. None of the irregular magnetites displayed rectangular or hexagonal projections at any tilt angles. They comprised ~66% of the total population and had a mean size of ~33 × 26 nm (Table A1). The irregular magnetites showed a range of W/L ratios from 0.3 to 1.0 (mean 0.8; Table A1).

Most magnetites in all morphological categories were free of crystallographic defects, although several irregular and whisker crystals were twinned (Fig. 4). Genetic inferences cannot be made from twinning because this phenomenon has been reported both from a variety of magnetotactic bacteria (e.g., Mann et al., 1984b; Bazylinski and Moskowitz, 1997) and from inorganically produced magnetite (Schwertmann and Cornell, 1991; Cornell and Schwertmann, 1996).

Approximately 90% of the magnetite crystals in the carbonate globules of ALH84001 were located in the rims of the carbonate globules; these rims are composed of randomly oriented crystals of carbonate that are as small as 10 nanometers in the longest direction (Fig. 5). We did not observe epitaxial relationships between these tiny carbonate crystals and magnetite particles within the globule rims as previously reported by Bradley et al. (1998).

4.1.4. Magnetite Crystals from Magnetotactic Bacteria

For comparison, we studied size, shape, and W/L ratios for magnetite crystals from cells of the marine magnetotactic bacterium, strain MV-1 (Table A1; Figs. 3k–r and 6). In addition, data reported in the literature are shown for magnetites from magnetotactic bacteria strains MV-1, MV-2, and MC-1 (Table A1; Sparks et al., 1990; Meldrum et al., 1993a; b). The mean size of MV-1 particles in our study was 42 nm × 30 nm (Table A1). We included in these measurements the dimensions of the smaller magnetite particles found at the ends of chains, which are interpreted as being immature superparamagnetic crystals. MV-1 particles displayed a hexagonal, a rectangular, or a diamond outline at various tilt angles (Figs. 3l–r and 6). In certain orientations, MV-1 crystals with rectangular projections displayed faceted ends on opposing corners (Figs. 3p–r). The mean W/L ratio for MV-1 crystals in our sample was 0.7 (Table A1); W/L ratios for elongated prismatic magnetite from bacteria strains MV-1, MV-2, and MC-1 reported in other studies (Sparks et al., 1990; Meldrum et al., 1993a; b; Devouard et al., 1998) were all between 0.6 and 0.8 (Table A1). No elongated prismatic magnetite crystals from any of these bacterial strains had W/L ratios < 0.3, with the exception of biogenic, needle-like magnetite crystals with axial ratios of ~0.1 described by Vali and Kirschvink (1991).

4.1.5. Selected Inorganic and Biogenic Extracellular Magnetite Crystals

Size, shape and W/L ratios for commercially produced inorganic magnetite (Nanophase™; Fig. 7), biogenic extracellularly produced magnetite (Zhang et al., 1998), and inorganically precipitated magnetite particles (Schwertmann and Cornell, 1991) are reported in Table A1. The W/L ratio for these groups is ~1, as most of the particles are equidimensional with rounded, hexagonal, or cubic outlines (Table A1). Morphology of the commercially produced magnetites showed rounded outlines (Figs. 7a,b); however, those that displayed hexagonal outlines at one angle also displayed those outlines when tilted (Figs. 7c-e). The geometric form likely represented by these particles is an icosahedron (Fig 7). The size distribution for inorganically produced magnetite measured previously (Schwertmann and Cornell, 1991; Cornell and Schwertmann, 1996; Devouard et al., 1998) shows a broader distribution than any of the intracellularly produced magnetite or the elongated prisms from ALH84001 and MV-1 (Table A1).

4.2. Chemical Composition

Based on the trace element concentrations (~400–500 ppm) in the NIST Glass Standard #610, we estimate that our minimum level of detection for Fe in a spectrum collected for 5000 sec. was ~150 ppm (Joy et al., 1986; Fig. 8a). We detected only very small (few hundred ppm level) but variable amounts of Si, P, and Mg in the acid-liberated elongated prismatic magnetite crystals (Figs. 8b,c). These elements were probably residual deposits from the acid dissolution and evaporation procedure. In spite of this, many grains were observed to be pure stoichiometric magnetite (Figs. 8d,e). Spectra of elongated prismatic particles analyzed in situ displayed significant amounts of Mg, Ca, Si, and P which we interpret as secondary x-rays generated from the surrounding grains (Fig. 8f); both Si and P appear to be associated with the carbonate (Fig. 5a).

In contrast, irregular and whisker magnetites, analyzed from both acid-extracted and in situ in the carbonates, commonly contained several hundred ppm of Al and/or Cr (Figs.9a-c). However, some irregular magnetites appeared to be stoichiometrically pure Fe_3O_4.

We analyzed biogenic magnetites from strain MV-1 and found them to be composed of only Fe and O. No other element present in the growth medium, including Ca, Cu, Co, Zn, Mo, Ni, Mg, Al, and Mn, were detected in these grains (Fig. 9d).

4.3. Statistical Analyses

Figure 10 shows the distribution of W/L ratios plotted against length for ALH84001 whisker, irregular, elongated prismatic magnetites and MV-1 elongated prisms. Overlaying the scatter plots are theoretically calculated curves for superparamagnetic-to-single-domain and single-domain-to-multidomain transitions in magnetite (Butler and Banerjee, 1975). Approximately 52% of the MV-1 magnetite crystals in our sample fell within the single-domain size, 16% in the transition range between single-domain and superparamagnetic, and 32% in the superparamagnetic range. Of the ALH84001 prismatic magnetites, 63% were in the single-domain size range, 20%

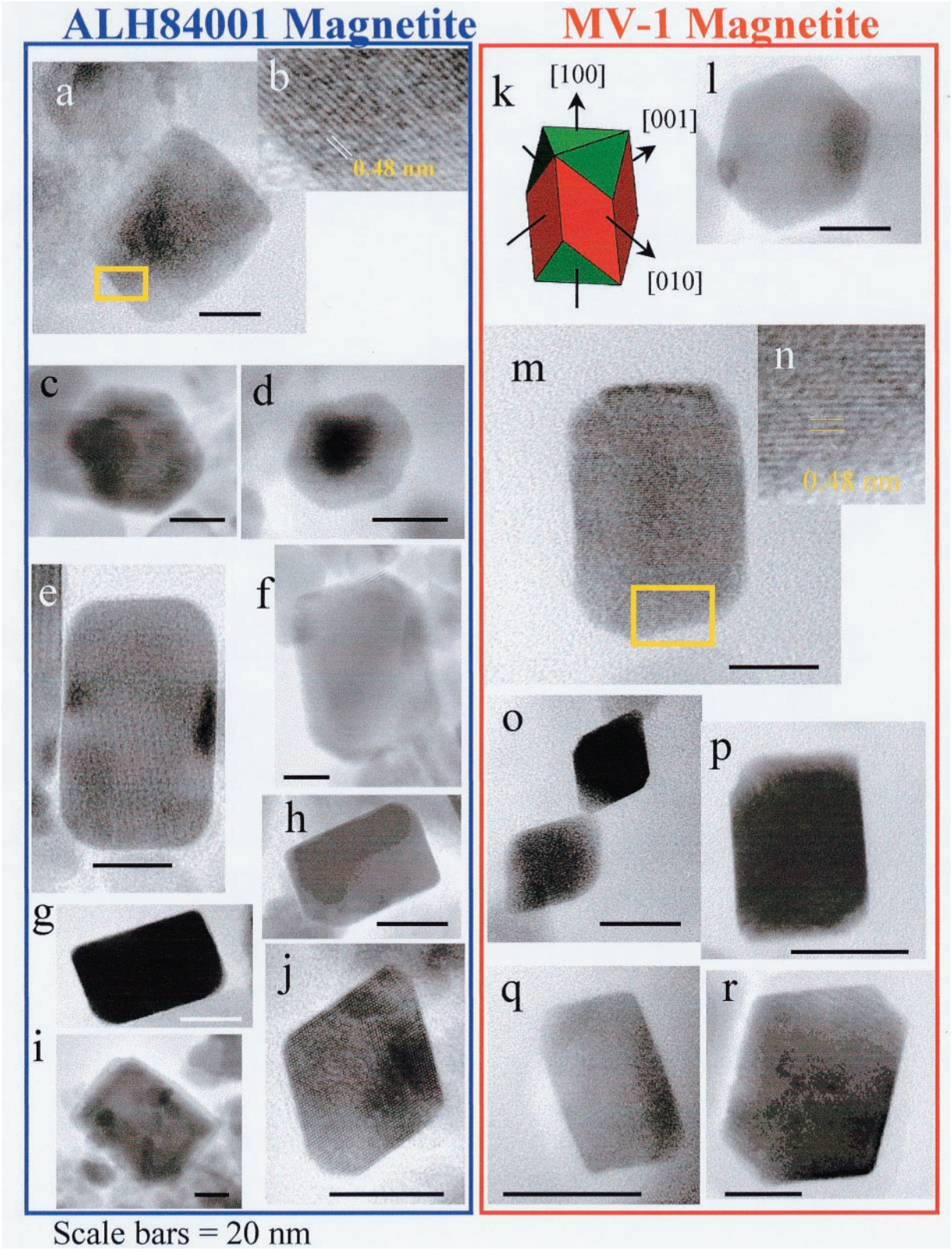
ALH84001 Magnetite
MV-1 Magnetite
a
b
0.48 nm
c
d
e
f
g
h
i
j
k
[100]
[001]
[010]
l
m
n
0.48 nm
o
p
q
r
Scale bars = 20 nm

Fig. 3. Comparison of ALH84001 elongated prismatic (a–j) and biogenic MV-1 (k–r) magnetite images at one angle (without corresponding tilted views); all scale bars equal 20 nm. (a,b) ALH84001 prismatic particles are elongated along the [111] direction as indicated by the lattice fringes (0.48 nm) which are at 90° to {111}; lattice fringes (0.48 nm) are consistent with magnetite {111}. Martian elongated prismatic magnetites display a variety of morphologies including hexagonal outlines (c,d), rectangular outlines (e–i), and diamond-shaped (j) outlines. Note faceted edges (i.e., imperfect rectangles) of some crystals (f,h,i). (k) Drawing after Mann et al. (1991) (also see Fig. 11f) of biogenic MV-1 magnetite crystals showing the hexagonal and rectangular views of the crystal at different orientations. MV-1 crystals show a variety of morphologies at given angles: (l) hexagonal outlines, (m,n) outline of a rectangular crystal stretched in the [111] direction (lattice fringes with 0.48 nm spacings are consistent with magnetite), (o) diamond-shaped and (p,q,r) rectangular outlines with faceted edges capping the elongated ends of the crystals. Note the faceted edges in (p) at the upper left and lower right corners; (q) and (r) also display faceted edges on opposing corners. The ALH84001 elongated prismatic magnetites are identical in size and morphology to biogenic magnetite produced by the magnetotactic bacterium strain MV-1.

were in the transition range, and 17% were in the superparamagnetic size range. Clearly, the majority of ALH84001 prismatic and MV-1 biogenic magnetites cluster in the single-domain region, but significant scatter occurs extending into the superparamagnetic range (Fig. 10b).

Caution is required when making such comparisons, because a correction for geometric distortions must be made when projecting a three-dimensional (3-D) object onto a two-dimensional (2-D) image plane (P. R. Buseck, private communication). TEM samples are analyzed by focusing an electron beam through the sample and onto an image plane. If a perfect cubic crystal has no preferred orientation in space, then the cube will project a range of 2-D geometric shapes dependent on the orientation of the crystal with respect to the image plane. When viewed along an edge, the cube will appear as a rectangle (W/L = 0.82); when viewed down a vertex, it will appear as a hexagon (W/L = 0.87); and when viewed perpendicular to one of its faces, it will appear as a square (W/L = 1.00). Consequently, it is difficult to identify crystal morphology and associated geometric properties from 2-D projections. In many cases, however, the geometry of a crystal can be predicted from the distributions of W/L ratios from 2-D projections. This procedure is valid provided the imaged crystals are represented by a single geometric shape and a sufficient number of measurements are made to compare the "true" distributions from "observed" W/L ratios of the 2-D plane images.

For the purposes of the following discussion, the term "observed" describes the experimentally measured properties of a system, while "true" describes the actual properties of the system. Therefore, the "observed" W/L ratio of a magnetite grain is derived from the measurements of the 2-D image data provided by the TEM while the "true" W/L refers to the actual 3-D W/L ratio. Deconvolving the data then becomes the means

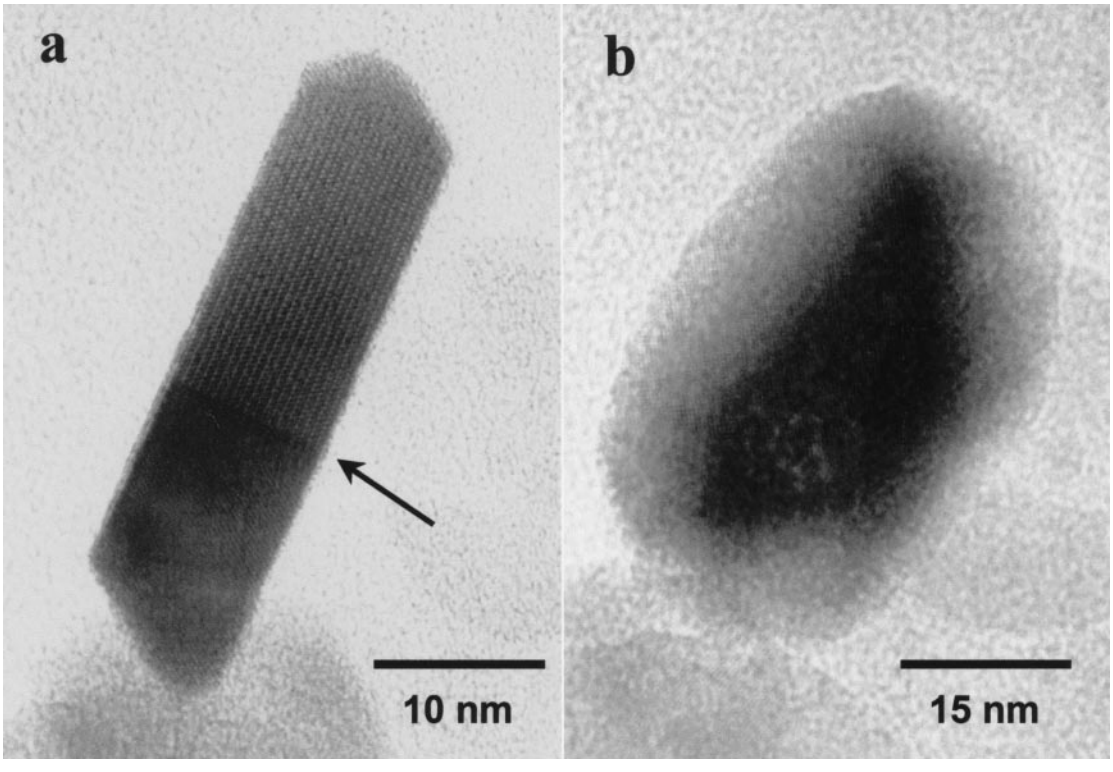

Fig. 4. A whisker from ALH84001 (a), which is a thin plate (b) at a different angle of rotation. The linear feature in the whisker indicated by the arrow is a spinel-law twin.

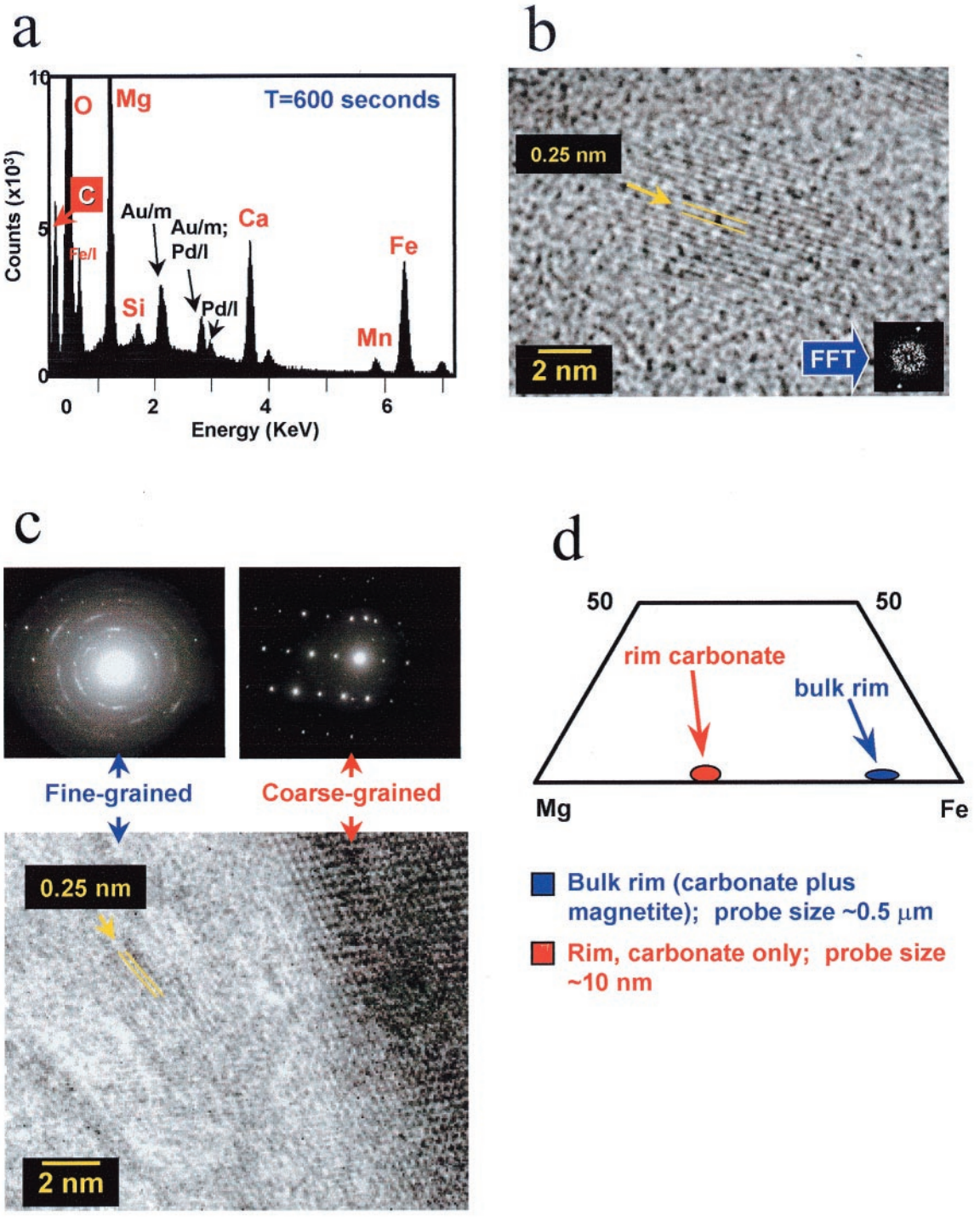

Fig. 5. ALH84001 carbonate globule rims are composed of fine-grained carbonate with embedded magnetite grains. (a) EDS spectrum of ALH84001 carbonate with major elements Mg, Fe, O, C, and Ca and minor Mn, and Si. Peaks from a conductive coating consisting of Au/Pd are also present. (b) High resolution image of a tiny carbonate crystal, with lattice fringes of 0.25 nm, is ~10 nm in the longest direction. The fine-grained nature of the carbonate in the rim precludes an epitaxial relationship forming between the magnetite and carbonate matrix. (c) a mixture of both fine-grained (diffuse rings and spots on the diffraction pattern) and coarse-grained ALH84001 carbonate. (d) TEM analyses of rim carbonate with and without contribution from magnetite. Mean composition (mole %) of fine-grained ALH84001 carbonate in a globule rim with ~60:40 Mg:Fe. Bulk analysis of the rim (carbonate and magnetite) approaches pure siderite (~10:90 Mg:Fe). However, pure siderite was not detected in either rim or interior regions of the globule.

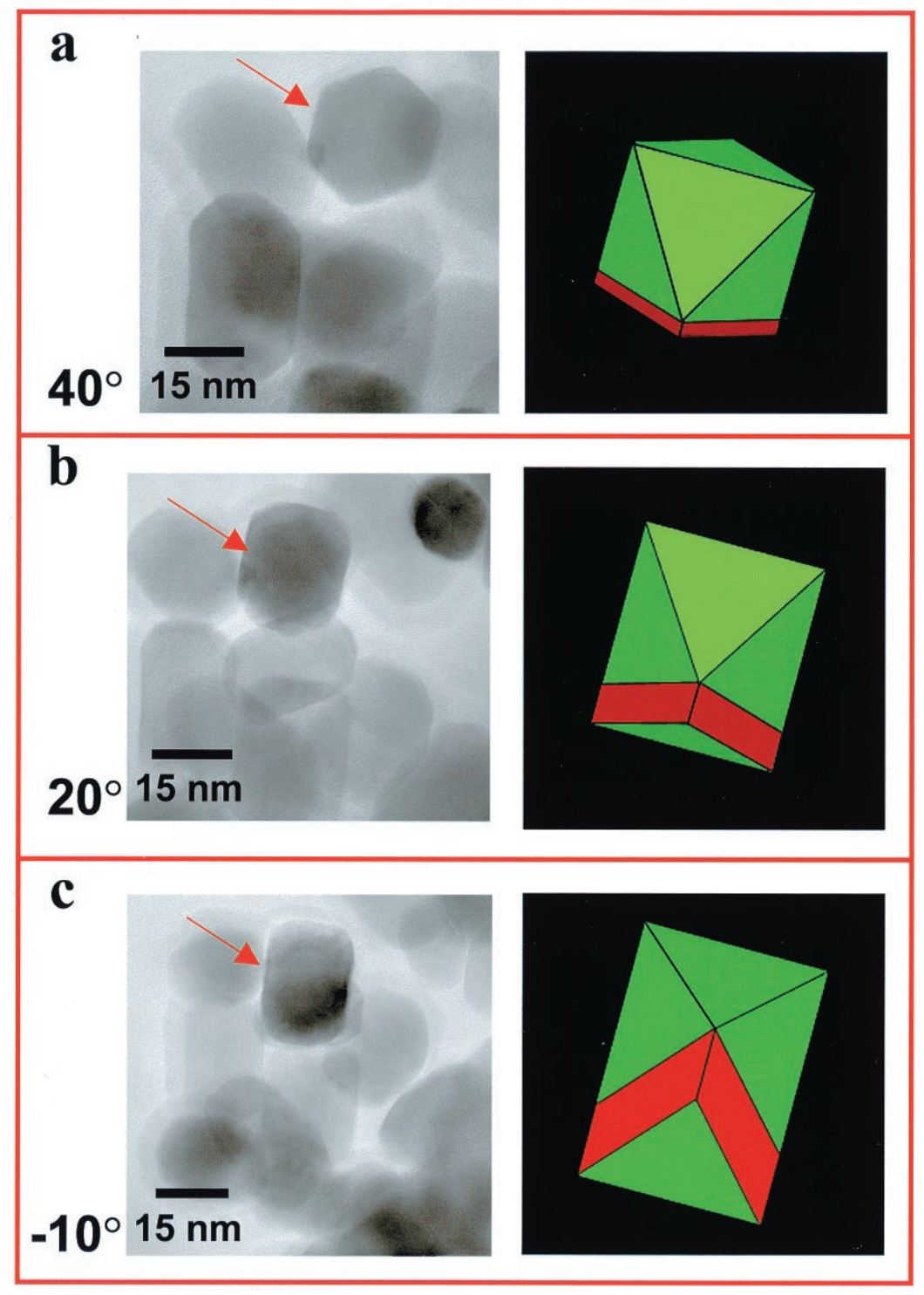

Fig. 6. Biogenic MV-1 elongated prismatic magnetite (red arrow) at three different angles of rotation. (a) The crystal has a hexagonal outline at +40°, a short rectangular outline at +20°, and a long rectangular outline at −10°. Green/red models are the corresponding two dimensional projections.

by which "observed" and "true" properties of the system can be correlated.

For example, consider the "true" geometry and physical characteristics of an elongated prism (e.g., MV-1 biogenic magnetite). TEM images of randomly aligned MV-1 magnetites have different morphologies at any given tilt angle, although the most common are hexagonal or rectangular image projections (Figs. 3 and 6). There are only two 3-D geometric

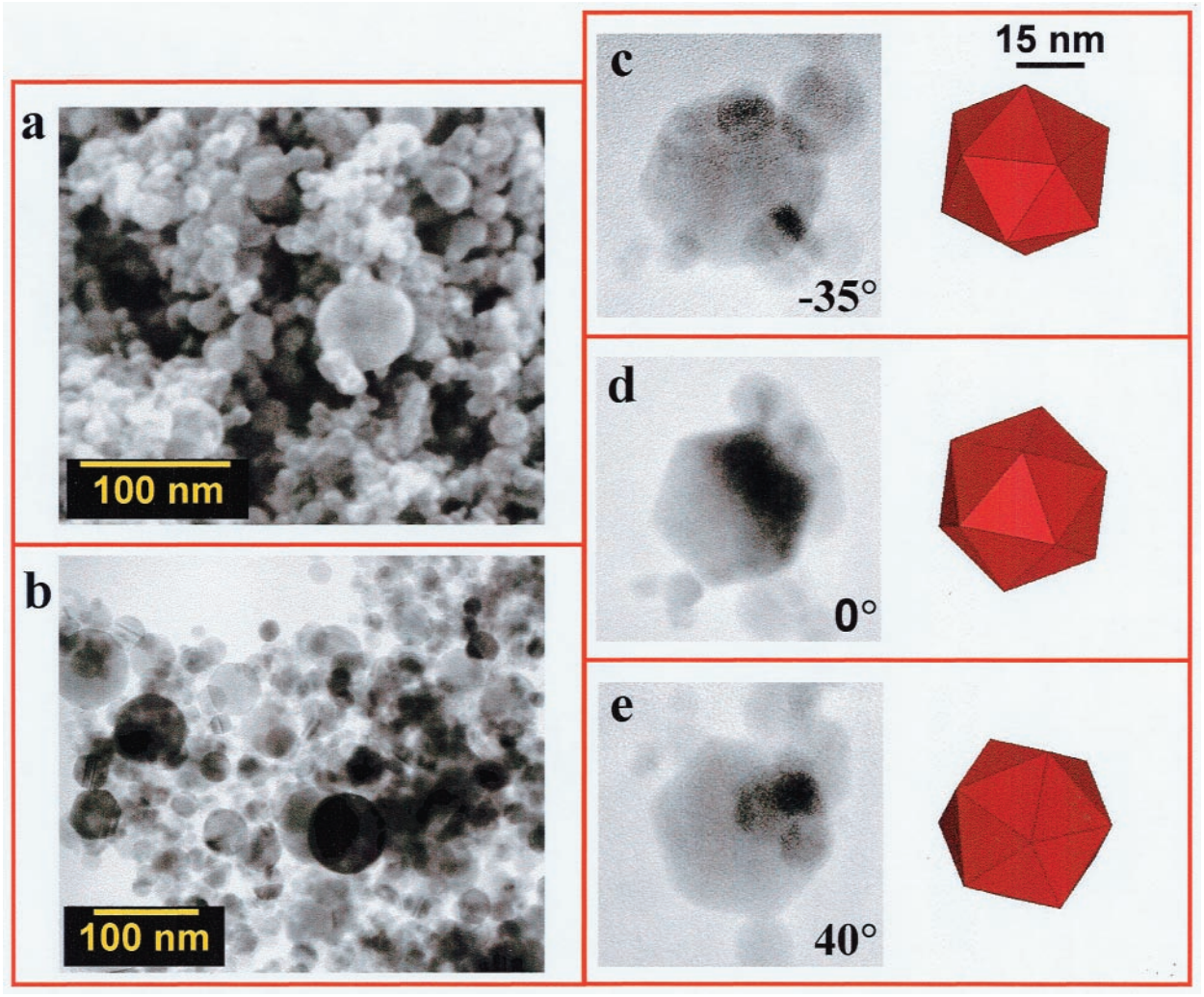

Fig. 7. Inorganic magnetite/maghemite crystals produced commercially by Nanophase™. (a,b) are SEM and TEM images of groups of crystals, respectively. Most particles are <100 nm in size and have spheroidal morphologies. (c–e) a single crystal with a hexagonal projection at three different angles of rotation (total 75° of tilt). This type of crystal has morphology similar to that of an icosahedron, a figure with twenty equivalent triangular surfaces that when projected in two dimensions typically displays a hexagonal projection (illustrated by the models). This morphology is unlike elongated prismatic magnetites from ALH84001 (Fig. 2) or MV-1 (Fig. 6).

shapes capable of producing exclusively hexagonal or rectangular 2-D projections (note: although an octahedron can be oriented such that it can produce a hexagonal and a rectangular projection, it will also give rise to many other projected geometries, and so it is excluded from further consideration). Therefore we can assume that the "true" geometry of the elongated prismatic MV-1 biogenic magnetite is constrained to be exclusively hexagonal or rectangular geometry or some close variation thereof.

If we measure the W/L ratios for a large number of magnetite grains having the same geometry ("observed"), we can construct a histogram that approximates some "global" 2-D W/L distribution. We use the term "global" because an experimentally "observed" W/L distribution is actually a composite of magnetite crystals having their own unique "true" W/L ratios (in 2-D projection, each crystal is capable of having its own unique "observed" W/L distribution). Therefore, the "observed" W/L distribution is a linear combination of unique 2-D projected W/L distributions of individual crystals. The geometry of a group of crystals has a distribution of W/L ratios that is unique. It is the distribution of these "true" W/L ratios we wish to determine.

Before we can proceed with the analysis, we must first calculate the "observed" 2-D W/L distributions generated from known 3-D geometric shapes. This can be accomplished using a Monte Carlo numerical computer simulation[2], in which we take geometric shapes defined in Euclidean space by an {x,y,z} Cartesian coordinate system and rotate them randomly. After rotation, one coordinate axis is collapsed producing a 2-D projection on the plane defined by the remaining two orthog-

[2] Code was written on a RedHat 6.1 Linux workstation using the GNU egcs-f77 compiler. Monte Carlo simulation utilized a modified long period [>2×1018] random number routine based on a L'Ecuyer generator with a Bays-Durham [reference "Numerical Recipes in Fortran 77" Press. W. H. Teukolsky, S. A., Vetterling, W. T., Flannery, B. P., Cambridge University Press (1992)].

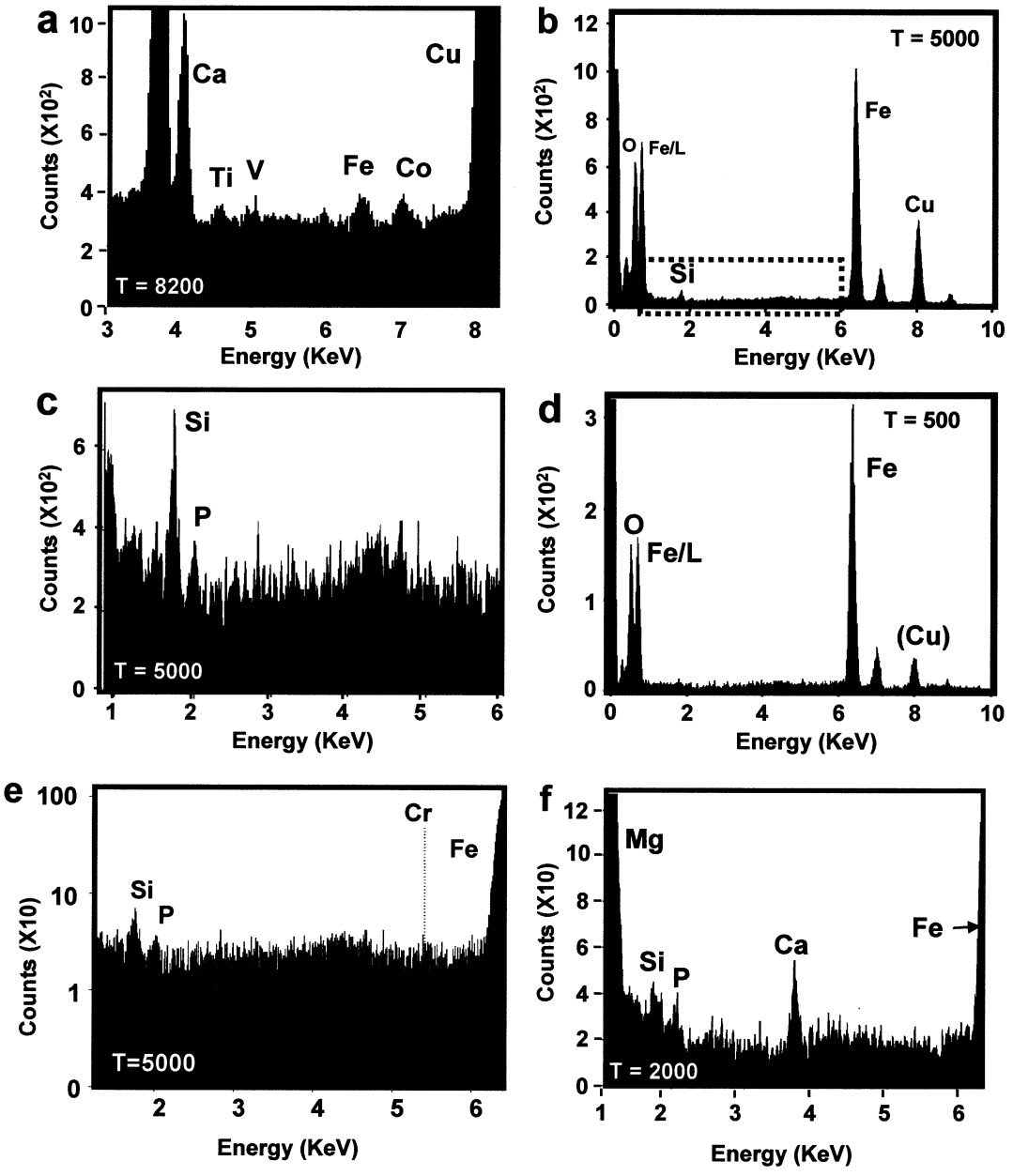

Fig. 8. (a) Energy dispersive X-ray spectroscopy (EDS) spectrum (3–8 KeV) of an ultramicrotomed Glass Standard #610 from the NIST; major elements are O, Si, Mg (not shown) and Ca. Copper is from the TEM support grid. Other trace elements (Ti, Fe, Co) are in the 400–500 ppm range; V is present in the standard in an unspecified amount. Time (in seconds) is shown in the lower left. (b) EDS spectrum of an acid-extracted elongated prismatic magnetite from ALH84001; it is mainly composed of Fe and O with trace Si. (c) An expanded view of (b) showing trace Si and P in the spectrum. (d) EDS spectrum of an acid-extracted elongated prismatic magnetite from ALH84001 with no minor or trace elements. (e) An expanded view (1–6 KeV) of an EDS spectrum of an acid-extracted Martian elongated prismatic magnetite. Dashed line indicates where a Cr peak would be if it were present at detectable levels. (f) ALH84001 elongated prismatic magnetite in situ with major Mg and Fe, minor Ca (all from the carbonate matrix) and trace Si and P. Si, in minor amounts, also appears associated with carbonate (also see Fig. 5a)

onal axes. This process is mathematically analogous to the observation of crystals by TEM.

In the context of hexagonal or cubic prisms we define the W/L ratio as the ratio between the maximum distance between any two vertices when projected on a 2-D plane perpendicular to the axis of elongation, and the maximum length between any two vertices when projected on a 2-D plane parallel to the elongation axis. For a given 3-D geometric object with a unique 3-D W/L ratio, there is a corresponding unique distribution of "observed" 2-D W/L ratios. We define the "observed" 2-D W/L ratio as the W/L ratio of the rectangle with the minimum area that completely encloses the projected image.

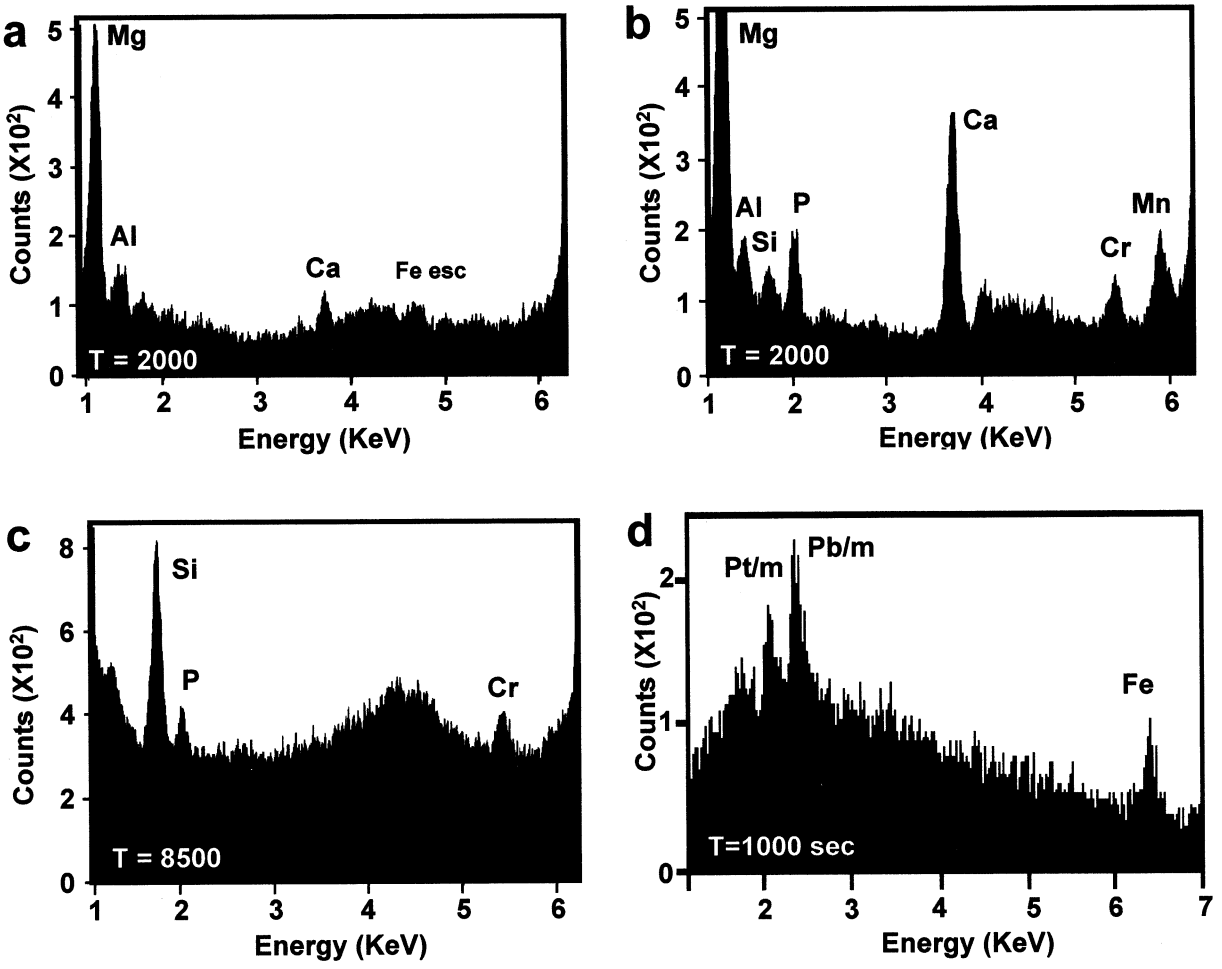

Fig. 9. ALH84001 irregular-shape and whisker magnetite grains have variable trace element compositions; occasionally irregular grains can have pure compositions similar to the composition of the Martian elongated prismatic grains (Fig. 8). Typically, irregular and whisker magnetite contain trace Al and/or Cr. (a) EDS spectrum of an irregularly shaped Martian magnetite crystal in situ with major Mg and minor Ca (from the carbonate matrix); trace Al is detected in the magnetite crystal. (b) EDS spectrum of an irregular Martian magnetite crystal in situ, with major Mg and minor Ca and Mn (from the carbonate matrix); trace Si, P, Cr, and Al are detected. Al and Cr are most likely in the magnetite; P is likely associated with the carbonate matrix. The source of the Si x-rays is uncertain although it is detected in situ in the carbonate globules (Fig 5a). (c) EDS spectrum of an acid-extracted irregular Martian magnetite, with trace Cr; the Si and P are most likely traces from the orthopyroxene matrix and apatite ($Ca_5(PO_4)_3$) grains in the ALH84001 meteorite. (d) EDS spectrum of magnetite grains extracted from strain MV-1 bacteria analyzed with a JEOL 6340 FEGSEM. Individual grains were placed on a brass stub and etched with atomic oxygen to remove all residual cellular debris (e.g., Na, Cl, K, etc.) that would otherwise be detected. These grains were coated with 2-nm Pt coating. Only Fe is from the magnetite, Pt is from the conductive coating, and Pb is from the brass substrate. No Al or Cr are detected in these biogenic magnetite crystals (compare with ALH84001 elongated prismatic particles Figs. 8b–f).

Given a limited number of experimental TEM measurements, we must approximate the "global" 2-D W/L distribution. To approximate this distribution, all possible W/L ratios (i.e., 0 to 1), for grains observed at different tilt angles, are determined using 20 bins, each 0.05 wide. Since an "observed" W/L distribution is represented by only 20 data points, we can only use a maximum of 20 adjustable parameters to fit this distribution.

For both hexagonal prisms and cubic geometries, using the described numerical Monte Carlo simulation, we calculated twenty 2-D W/L distributions. Each distribution represents the averaged W/L distribution generated from the 2-D projections, of a given geometry, whose "true" 3-D W/L ratio is randomly selected and falls within the following ranges:

$$\Psi_1 = 0 \Leftrightarrow 0.05 \ldots \Psi_2 = 0.05 \Leftrightarrow 0.1 \ldots \Psi_3 = 0.1 \Leftrightarrow 0.15 \ldots \Psi_{20} = 0.95 \Leftrightarrow 1$$

These 20 distributions form a basis set to describe the experimentally observed distribution. That is,

$$(W/L)_{observed} \cong \sum_{x=1}^{x=n} A_x \cdot \Psi_x$$

where A_x are the term coefficients of the 20 calculated 2-D W/L distributions. The optimal values for A_x can then be determined

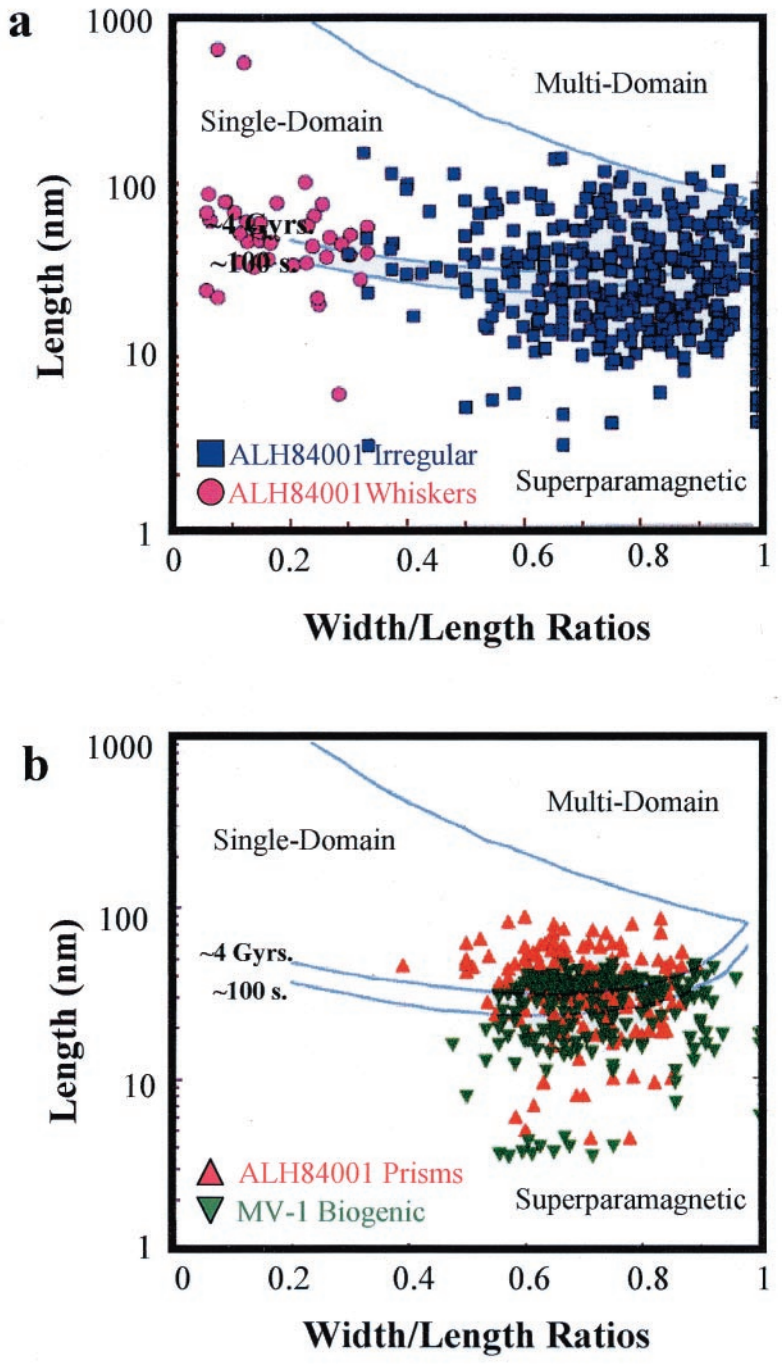

Fig. 10. Size and shape distributions of ALH84001 irregular and whisker magnetites (a) and ALH84001 elongated prismatic and biogenic MV-1 magnetites (b). Scatter plots (after Butler and Banerjee, 1975) illustrating the distribution of W/L ratios of individual magnetites as a function of length along their longest dimension. In such graphs, magnetites with cubic geometry lie to the right hand side of the plot whereas elongated whiskers lie to the left-hand side. Overlying the scatter plots are the theoretically calculated superparamagnetic-to-single-domain-to-multi-domain transition curves for pure, defect free magnetite crystals at 17° C. The uppermost curve represents the transition from single-domain to multi-domain, while the lower two curves represent the transition from superparamagnetic to single-domain behavior with half-lives, τ, of 100 sec. and 4×10^9 years (see Butler and Banerjee, 1975, for a complete discussion). Note the separation of the whisker magnetite from all other magnetite groups.

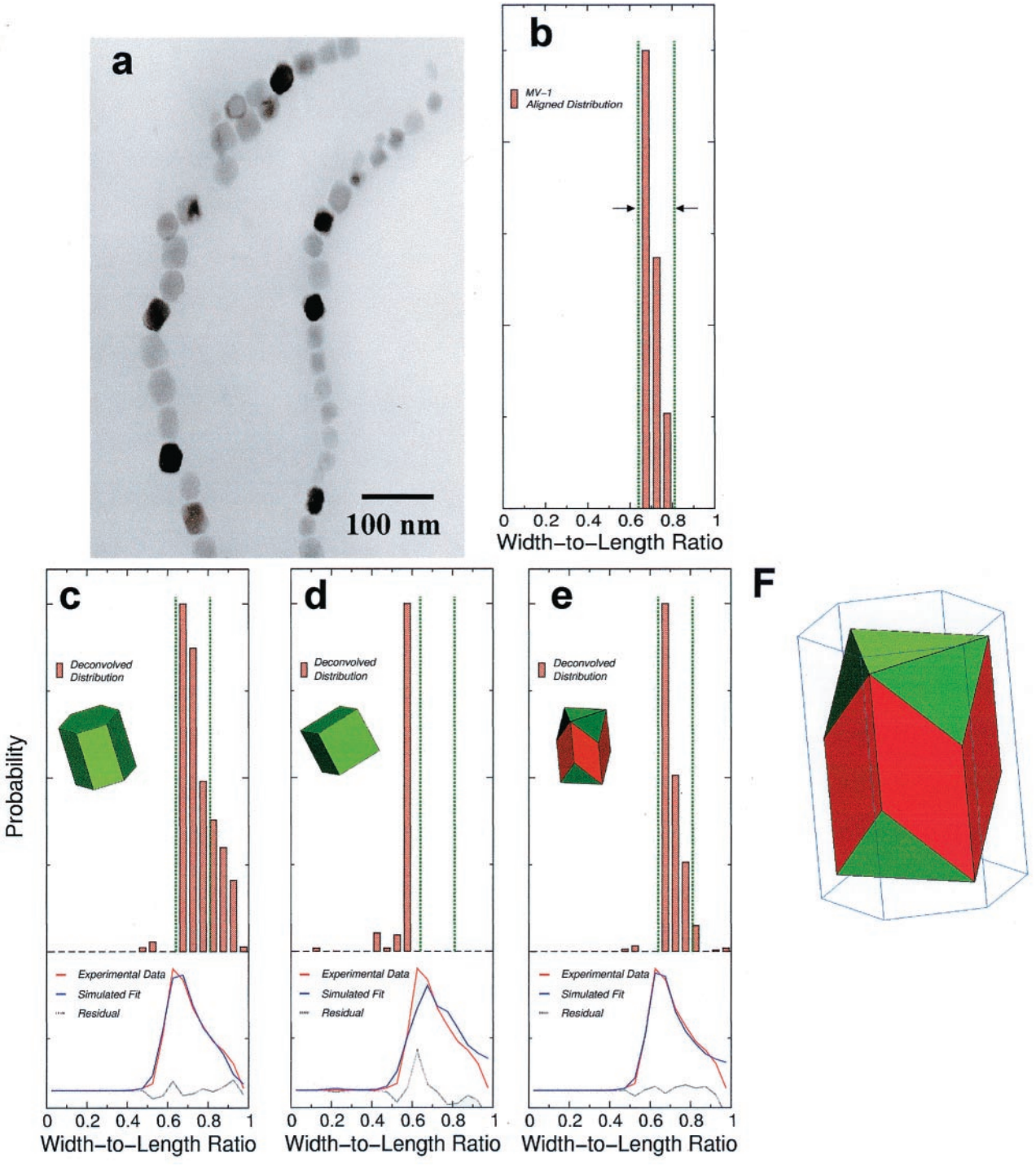

Fig. 11. Comparison of the true W/L distribution of MV-1 biogenic magnetites with the calculated distributions (b-e) obtained through a numerical deconvolution procedure that takes as input the 2-D image projections of randomly oriented magnetites. TEM image (a) shows aligned biogenic magnetites within individual cells of the MV-1 strain of magnetotactic bacteria. The magnetite elongation axis in this image is constrained perpendicular to the imaging plane. (b) is the histogram of the individual W/L ratios determined from (a) and shows a narrowly constrained W/L distribution that lies between W/L $\sim$ 0.68 and W/L $\sim$ 0.80, indicated by the dashed vertical lines. (c-e) show the deconvolved W/L distributions calculated from randomly oriented MV-1 magnetites after correction for geometric projection errors. In (c) the geometry of the magnetite crystals is assumed to be hexagonal prisms, while in (d) they are assumed to be cubes. Neither distribution reproduces the true W/L distribution as measured in (b). In (e), however, a modified hexagonal prism geometry is used; and, within experimental error, this geometry does correctly reproduce the true W/L distribution. Below each of the deconvolved distributions are the experimentally measured data and the corresponding simulated fit that would be observed under the same experimental conditions. The residual represents the difference between the experimental and simulated curves. (f) Idealized drawing of a mature magnetite crystal produced by magnetotactic bacteria strain MV-1 initially described by Mann et al. 1991). Equivalent {111} faces are shown in green and equivalent {110} faces are shown in red. The correct mathematical term for this type of crystal is a hexaoctahedron (completely discussed in the text). Note the faceted edges on the elongated ends of this crystal that constrains the deconvolved W/L distribution as shown in (e).

using a nonlinear optimization algorithm, in which A_x coefficients are treated as adjustable parameters. In such a nonlinear optimization we minimize the function:

$$[(W/L)_{observed} - \sum_{x=1}^{x=20} A_x \cdot \Psi_x]^2 \Rightarrow 0$$

subject to the constraint that all adjustable parameters, A_1, A_2, . . . A_{20}, must be greater than or equal to zero[3].

An analysis of MV-1 magnetite provides a model to validate and refine our deconvolution process. We determined the distribution of aligned magnetites within MV-1 cells where the elongation axis of the magnetite crystals is known to lie parallel to the TEM grid (Fig. 11a). In this situation, the "observed" 2-D W/L projection distribution has a one-to-one correspondence with the "true" 3-D W/L distribution. Using an elongated prismatic geometry, the deconvolution approach should match the aligned image data perfectly. Figures 11a,b show a TEM image of aligned MV-1 magnetites and the corresponding "true" 3-D W/L ratio distributions.

The distribution of aligned MV-1 particles (Fig. 11b) only partially correlates with those calculated using a hexagonal prism (Fig. 11c) or cubic geometry (Fig. 11d). In the case of cubic geometry, the deconvolved "true" 3-D W/L distribution is centered at a W/L ratio significantly lower than the aligned image data and has a dissimilar distribution (Fig. 11d). Clearly MV-1 magnetites cannot accurately be represented as having cubic geometry. For hexagonal prisms, the deconvolved "true" W/L distribution is centered closely with the aligned image data but does show a greater spread in the distribution (Fig. 11c). Extensive Monte Carlo simulations combined with subsequent deconvolution using modified hexagonal prism geometries indicates that the width of the deconvolved distribution can be decreased by effectively "rounding" off the ends of hexagonal prisms.

Detailed TEM observation of individual MV-1 magnetites shows that the ends of each crystal are faceted on alternate vertices; each end face has threefold rotational symmetry about the elongation axis. The facets at one end are rotationally offset from the facets at the other end by $\pi/3$ radians. The resulting deconvolution of randomly oriented MV-1 crystals using this geometry is shown in Figures 11e and 12a. This morphology for MV-1 crystals was first suggested by Mann et al. (1991) (Figs. 3k and 11f). Clearly, within experimental error and simulation approximations, the deconvolved distribution of elongated prisms with faceted ends (Figs. 11e and 12a) is identical to that of the aligned image data (Fig. 11b). The nature of the "observed" 2-D distribution is a sensitive indicator of the 3-D crystal geometry. This point is key when applying this deconvolution process to the ALH84001 prisms.

Like MV-1, TEM images of individual ALH84001 prismatic magnetites show either approximately hexagonal or approximately cubic projections, suggesting that the underlying 3-D crystal geometry is either hexagonal prisms or cubes. Recalling that the assumed geometry strongly influences the deconvolution results, it is essential to accurately define this geometry before attempting deconvolution. Fortunately, detailed TEM images of individual ALH84001 prismatic magnetites under incremental stage rotation bear a striking resemblance to the images of MV-1 magnetites. In fact, it is not possible to distinguish between TEM images of MV-1 and of ALH84001 prismatic magnetites. Therefore, we use the same geometric model for deconvolving the ALH84001 prismatic and MV-1 magnetites. Figure 12b summarizes the results of the deconvolution for ALH84001 prismatic magnetites.

Because the deconvolved W/L distributions of both MV-1 and ALH84001 prismatic magnetites are narrow (Figs. 12a,b), we can approximate the distribution with a single W/L ratio of 0.675 for MV-1 and 0.725 for ALH84001 prismatic magnetites. The deconvolution procedure for length is directly analogous to that already outlined for the W/L ratio. Figures 12c,d show the results of deconvolving the experimentally measured length distributions of MV-1 and ALH84001 prismatic magnetites. These length distributions are narrower than expected for log-normal[4].

Size distributions for magnetite crystals produced by simple inorganic growth processes are log-normal (Nicholls, 1987); this is apparent in the data of Devouard et al. (1998). Deviations from this log-normal distribution requires that the growth not be characterized by an independent, identically distributed, random process of single-atom addition (i.e., any situation where atoms are randomly being added to a crystal surface, including tiny crystals growing in aqueous solution or even particles being deposited from a high-temperature vapor phase). In the case of magnetotactic bacteria, this size distribution is truncated when the growing magnetite crystals contact the magnetosome membrane, which inhibits further diffusion of cations to the growing surfaces (Fig. 12d). Because the size and shape of the magnetite crystals are under genetic control, natural selection for magnetotaxis can stop crystal growth before it reaches the multi-domain size, yielding a distinct truncation in the size distribution. This cutoff is also present in the elongated prismatic fraction of the ALH84001 magnetites (Fig. 12c).

[3] Deconvolution procedure used an adaptive non-linear least squares algorithm with linearly constrained optimization [reference "The Port Mathematical Subroutine Library" Ed. Phylis A. Fox, AT&T Bell Telephone Laboratories. Inc. (1984)].

[4] Most crystal growth processes produce a log-normal size distribution because the probability of a crystal with *n-I* atoms growing to a particle of size *n* depends first upon the particle having reached size *n-I*. Given the stochastic nature of diffusive processes, the addition of each new atom can be viewed as a random, identically distributed, independent process. Hence, the probability of a crystal reaching size *n*, $P(n)$, is given by:

$$P(n) = \prod_{x=1}^{x=n-1} P(n-x) \Rightarrow \ln[P(n)] \propto \sum_{x=1}^{x=n-1} \ln[P(n-x)]$$

Since the log of a random variable is also a random variable, each *ln(P(n−x))* is also a random identically distributed, independent variable. The *Central Limit Theorem* says that under fairly general conditions that the sum of a large number of independent and identically distributed variables is approximately normally distributed. Hence, in the simple case of crystal growth by single atom addition, the size distribution *P(n)* ought to have a log-normal distribution.

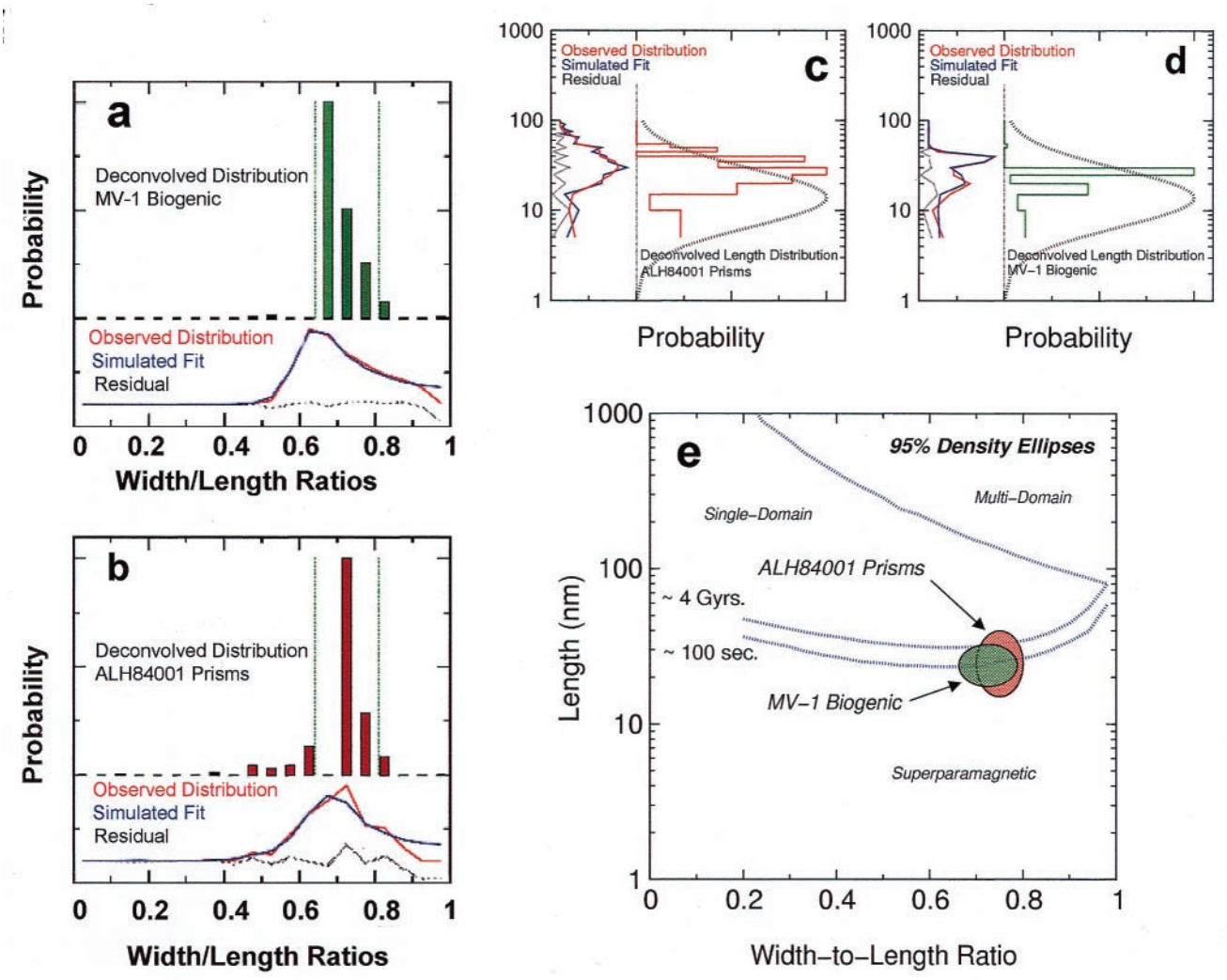

Fig. 12. Deconvolved W/L and length (L) distributions calculated from randomly oriented MV-1 biogenic and ALH84001 prismatic magnetites. (a,b) show the deconvolved W/L distributions for MV-1 and ALH84001, respectively. MV-1 magnetites are characterized by a highly constrained distribution whose limits are indicated by the dashed vertical lines. ALH84001 magnetites are also characterized by a similar highly constrained distribution. In both cases the deconvolution procedure uses a modified hexagonal prism geometry with faceted ends as a model for the numerical Monte-Carlo simulations that are used to correct for geometric projection errors. Note that the distributions for randomly oriented MV-1 magnetites (a) are identical within experimental error to both the distribution of aligned MV-1 magnetites (11b) and mathematically corrected distribution of elongated prisms with faceted ends (11e). Below each deconvolved histogram are the experimental measured data and the calculated simulated fit that would be observed from the deconvolved distribution if measured under same experimental conditions. The residual is the difference between the two distributions. Deconvolved L distributions for MV-1 (c) and ALH84001 prismatic (d) magnetites using the same geometric model as described above. Again, shown below each deconvolved distribution is experimental measured data, the calculated simulated fit and the resulting residual. The 90% density ellipses for MV-1 and ALH84001 prismatic magnetites (e) are shown on a W/L versus L plot calculated using the deconvolved distributions from (a-d). Overlaid on this plot are the theoretical transition lines for single-domain-to-multidomain behavior and superparamagnetite-to-single-domain behavior at 17°C with half-lives of 4×10^9 years and 100 sec. (see Butler and Banerjee, 1975, for complete discussion).

Using the deconvolved data provided in Figure 12, we can construct the true W/L versus length graphs for MV-1 biogenic and ALH84001 prismatic magnetites (Fig. 12e). Both MV-1 and ALH84001 prismatic magnetites lie at the intersection of the superparamagnetic and single-domain regimes. In the case of MV-1, this observation is consistent with the hypothesis that magnetotactic bacteria will grow magnetites in a controlled manner up to the point at which they cross the transition from superparamagnetic to single-domain behavior.

In short, based on these statistical analyses, MV-1 and ALH84001 prismatic magnetite particles have indistinguishable crystal geometries, highly restricted W/L ratios, restricted anisotropic length distributions, and size distributions that lie in the superparamagnetic to single-domain region.

5. DISCUSSION

5.1. Comparison of ALH84001 Magnetite with Terrestrial, Extraterrestrial, and Synthetically Produced Magnetite

Magnetite is found in many rock types on earth and in meteorites (see selected references in Tables A2–A6). We have assembled a wide variety of published literature on magnetite found in rocks from high-temperature (Table A2), hydrothermal (Table A3), and low-temperature (Table A4) terrestrial environments, magnetite in extraterrestrial samples (Table A5), and synthetically and biogenic extracellularly produced magnetite (Table A6).

5.1.1.High-Temperature

Magnetite crystals in igneous and metamorphic rocks are inorganically produced and have a highly variable size distribution, morphology, and chemical composition (Table A2). The smallest magnetite crystals (2–10 nm) are found in volcanic glass (Table A2; e.g., Schlinger and Smith, 1986; Schlinger et al., 1988; Itoh et al., 1989; Heider et al., 1993; Pick and Tauxe, 1994); and some of the larger magnetite grains (mm) are found in carbonatites (Table A2; e.g., Moecher et al., 1997) and in feeder dikes in dendritic and columnar forms (tens of mm; Table A2; e.g., Nystrom and Hendriquez, 1994). Although magnetite commonly occurs as octahedral crystals, unusual elongated and platelet-shaped forms ranging from ~100 nm to tens of μm, typically contain Ti, Al, and/or V (Table A2; e.g., Morgan and Smith, 1981; Geissman et al., 1988). Magnetite in metamorphic and igneous rocks is typically not pure and contains other minor elements such as Ti, V, Al, and Cr (Table A2). Most magnetite in metamorphic and igneous rocks is not in the single-domain size range, although some fine-grained, single-domain magnetite has been found embedded in volcanic glasses, certain anorthositic rocks, and other igneous silicates (Table A2). Most single-domain magnetite from these sources contains some Ti. The few examples of chemically pure magnetite described in the literature include <20 nm-sized, superparamagnetic crystals in glass (Table A2; Schlinger and Smith, 1986; Lawson et al., 1987; Schlinger et al., 1988) and 50–1200 m-sized grains in Archaean gneiss (Table A2; Benn et al., 1993).

5.1.2. Hydrothermal

Magnetite in preexisting rocks can experience alteration by fluids at moderate (<300°C) or elevated temperatures, producing recrystallized magnetite (Table A3). Rims of magnetite on ilmenite (Abzalov, 1998; Borrok et al., 1998); coarse-grained octahedral magnetite (Stenina et al., 1979; Rhodes et al., 1997); very fine-grained magnetite crystals (e.g., Van der Hoeven et al., 1999); and dendritic and cruciforms of magnetite (Van der Voo et al., 1993) have been described (Table A3). Recrystallized magnetite commonly contains other elements such as Ti, Al, Si, Mg, and Mn (Table 3).

5.1.3. Low-Temperature

Terrestrial magnetite is reported extensively from low-temperature, carbonate-rich environments, including limestones, carbonate oozes, sediments, and soils (Table A4). Previous work indicates that these magnetites may originate by biological and inorganic processes (Table A4); it is common to see both inorganic magnetite particles with a wide size distribution and biogenic, single-domain magnetites with a narrow size distribution within the same sample (Table A4). Low temperature alteration of preexisting minerals (e.g. pyrite, FeS_2) can result in botryoidal, spherical framboidal, and irregularly shaped magnetite (Table A4; e.g., Jackson et al., 1988; Suk et al., 1990a; Suk et al., 1991). The interaction of oxidized iron minerals with hydrocarbons may produce magnetite with spherical or irregular shapes, ranging from ~20 nm to several hundred μm (Table A4; e.g., Elmore et al., 1987; McCabe et al., 1987; Kilgore and Elmore, 1989; Elmore and Crawford, 1990; Schwartz et al., 1997). Magnetite in soils may have formed by a variety of processes (e.g., authigenic, biogenic; Table A4; Sidhu et al., 1980; Taylor, 1981; Fassbinder et al., 1990).

5.1.4. Extraterrestrial Sources of Magnetite

Magnetite crystals in non-Martian meteorites are generally much larger than the single-domain size range and are not chemically pure (see Table A5). Single-domain magnetite in interplanetary dust particles (IDPs) has an irregular morphology and typically contains trace amounts of Cr (Table A5; Keller et al., 1992b). Magnetite rims, composed of well-crystallized grains, form on the exteriors of IDPs that have been heated during atmospheric entry (Table A5; Keller et al., 1992a). Nanometer-sized magnetites are also dispersed in phyllosilicate-rich regions of some heated IDPs (Keller et al., 1992a).

5.1.5. Synthetically and Biogenic Extracellularly Produced Magnetites

Magnetites precipitated inorganically at low temperatures do not exhibit the specific and unusual characteristics of magnetites produced by magnetotactic bacteria. While it is possible to grow pure magnetite crystals inorganically at low temperature from aqueous solutions containing Fe as the only cation (Table A6; Schwertmann and Cornell, 1991; 1996), natural solutions commonly contain other cations, such as Ti, Al, Mn, Cu, and Cr, that co-precipitate in the magnetite structure (Table A5). These substitutions occur readily at low temperature (e.g. Al; Table A6; Schwertmann and Murad, 1990), and these magnetite crystals also range considerably in size and typically display octahedral and cubo-octahedral morphologies (Table A6). Other magnetite morphologies produced experimentally include rod-shaped, with an average size of 80 nm in length, produced at temperatures < 150°C (Table A6; Yitai et al., 1994) and whisker-like, produced at 65–100°C (Table A6; Wang et al., 1998).

Magnetite crystals produced extracellularly as a byproduct of bacterial iron reduction by dissimilatory iron-reducing bacteria (Table A6; Moskowitz et al., 1989; Sparks et al., 1990; Lovley; 1991; Zhang et al., 1998) do not show the fingerprints of strict genetic control and appear indistinguishable from some magnetites produced by inorganic processes.

5.1.6. ALH84001 Magnetites

Irregular magnetites do not share a simple geometric morphology, nor do they show a consistent chemical purity. Whisker magnetites do not show a consistent chemical purity, nor are they defect free. These observations indicate that neither population can collectively meet the six criteria for biogenicity previously outlined. Thus their use as a biosignature is not justified. Irregular and whisker-shaped magnetites have morphologies and chemical compositions that are consistent with some inorganically produced magnetites (Tables A2–A6). Alternative explanations are necessary to explain their origin and some possibilities are discussed below.

It is possible that the irregular and whisker magnetites formed by inorganic in situ and/or detrital processes (Golden et al., 1999; 2000; McSween Jr. and Harvey, 1998; Treiman and Romanek, 1998; Valley et al., 1997; Warren, 1998). Some of these crystals may display an epitaxial relationship with the surrounding matrix material. One example of such a process is described here. The precipitation of inorganic magnetite can occur in situ when a saturated solution rises along a pore in a substrate under capillary action and becomes supersaturated due to solvent evaporation (Givargizov, 1987). The fluid arranges itself in layers parallel with the walls and takes on an order reflecting that of the walls (Schoen and Diestler, 1987). While this effect decreases with increasing distance from the walls, it persists indefinitely in the fluid layer nearest the walls (Schoen and Diestler, 1987). When nucleation and subsequent crystal growth occur, these crystals may take many forms, including whiskers and/or plates (Givargizov, 1987), that have epitaxial relationships with the substrate.

If irregular and whisker ALH84001 magnetites form in the presence of fluids, and assuming that dissolution and crystallization occur slowly, only very small quantities of fluid are necessary at any given time. The same fluids can be used for dissolution, diffusion of components within a closed system, and crystallization of magnetite (Suk et al., 1993a). For example, the Cr and Al commonly observed in the irregular and whisker magnetite populations could have come from minor dissolution of chromite [(Mg, Fe, Al)Cr_2O_4], also previously reported in the ALH84001 meteorite (average Al_2O_3 is 8.53 wt.% in ALH84001 chromites; Mittlefehldt, 1994). Both of these elements can be incorporated into the inverse spinel structure of magnetite at low temperatures; this is often observed in a terrestrial context (Tables A3 and A5).

Even though it has been suggested that magnetites in ALH84001 formed by a high-temperature event (e.g., shock; Scott et al., 1998), this would not explain the presence of Al and/or Cr in some of the irregular and whisker magnetites. Under the high-temperature hypothesis, the irregular and whisker magnetites would have had to form in situ in the carbonate by its thermal decomposition. There are, however, no reports of either Al or Cr in the carbonate of the globules (Mittlefehldt, 1994) because these elements do not precipitate in carbonate (Veizer, 1983).

For the fraction of irregular and whisker magnetites with pure composition, a thermal decomposition origin cannot be excluded, although it would require a series of well-constrained events not outlined here. The difficulty of accepting this hypothesis is that the ALH84001 carbonate globules are composed primarily of Fe-poor to Fe-bearing magnesite ($MgCO_3$) with minor amounts of Ca and Mn (McKay et al., 1996; Mittlefehldt, 1994; Harvey and McSween, 1996). Therefore, magnetite produced by thermal decomposition of globules with this composition should contain Mg and Mn in trace amounts and so would not be pure in composition. Furthermore, carbonate in this region would show chemical evidence for Fe mobilization and none is observed.

A biogenic process cannot be completely ruled out for some of the chemically pure ALH84001 irregular and whisker magnetites; e.g., whisker-like magnetites have recently been identified in a magnetotactic bacterium (A. P. Taylor, private communication).

In a detrital origin, there would be few, if any, constraints on the origin of the irregular and whisker magnetite crystals, and we do not examine this hypothesis further.

In contrast, the elongated prismatic ALH84001 magnetites show chemical and physical characteristics that have no analog in either the abiotic terrestrial or the extraterrestrial database (see below).

5.2. Comparison of ALH84001 and MV-1 Elongated Prismatic Magnetite

The elongated prismatic ALH84001 magnetites meet five of the six criteria that were previously defined to be characteristic of biogenic activity:

1. single-domain size and restricted anisotropic W/L ratios;
2. chemical purity;
3. crystallographic perfection;
5. an unusual morphology consistent with a hexaoctahedral geometry; and
6. elongation along the [111] axis.

The remaining property, that of magnetite chains (4.), cannot be addressed because the ALH84001 magnetites were extracted from the meteorite. Therefore, spatial relationships within the carbonate globules prior to acid-extraction are not preserved. Furthermore, as noted earlier, once a magnetotactic bacterium cell dies and decomposes, its magnetite chain collapses; only in rare instances are chains preserved in the rock record (Chang and Kirschvink, 1989). Because of this, we cannot evaluate whether the ALH84001 elongated prismatic magnetites were ever aligned in chains.

The Venn diagram shown in Figure 13 summarizes the criteria used for the identification of intracellularly produced biogenic magnetite. Although bacterial magnetite crystals produced by some common strains (e.g., equant cubo-octahedra crystals of *Magnetospirillum magnetotacticum*) fall outside the central area of the diagram, no inorganically produced population of magnetite crystals has yet been found which inhabits this central region. When these criteria are applied to magnetite in carbonate globules formed on Mars, the elongated prismatic ALH84001 crystals are indistinguishable from magnetite produced by terrestrial magnetotactic bacteria strain MV-1.

The large number of crystals in ALH84001 having identical elongated prismatic morphologies would also require controlled or steady growth conditions, which are seldom attained in natural abiotic or synthetic environments (Devouard et al., 1998; Tables A2 and A6). It is difficult to conceive of an

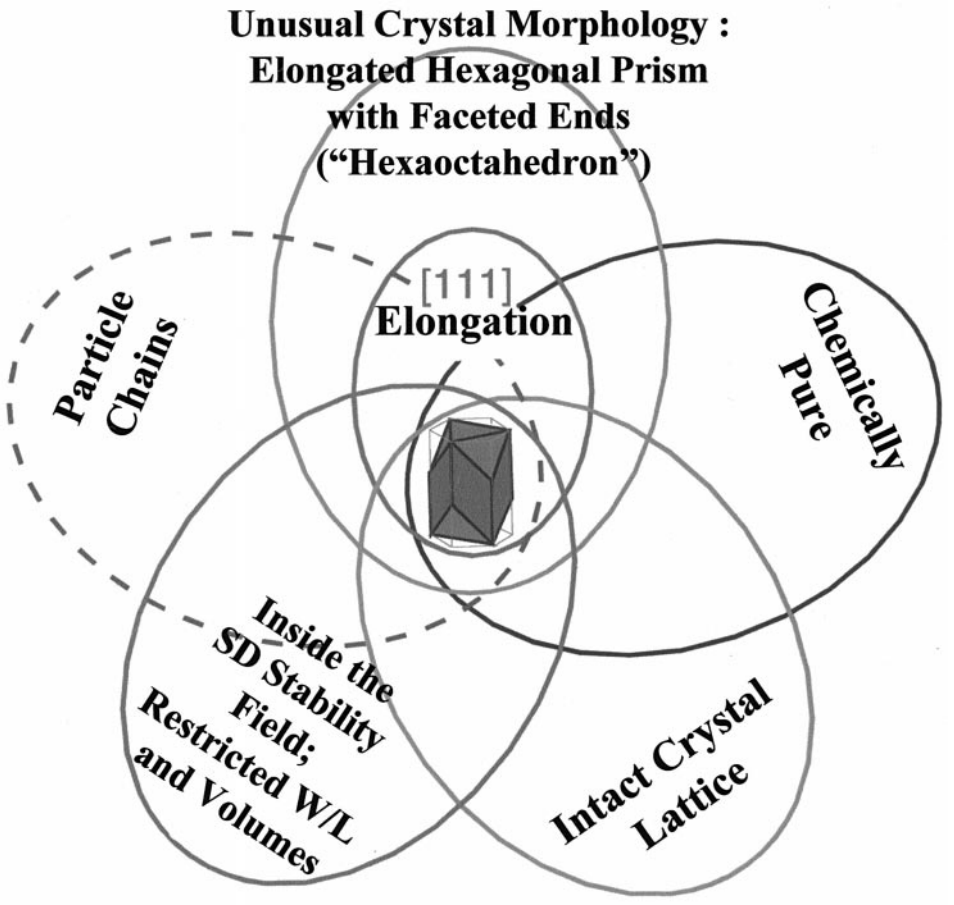

Fig. 13. The Venn diagram summarizes criteria used for identification of intracellularly produced biogenic magnetite. These criteria include unusual crystal morphology (e.g., elongated hexagonal prismatic magnetite with faceted ends produced by magnetotactic bacteria strain MV-1; this hexaoctahedral geometry is completely described in the text); chemically pure composition; an intact crystal lattice that is relatively free of defects (though it may occasionally have twinned crystals); restricted W/L ratios and volumes that place the crystals in the single-domain stability field; and occurrence in chains. All of these characteristics maximize the magnetic moments of the magnetite crystals. Although bacterial magnetite crystals produced by some common strains (e.g., equant cubo-octahedra crystals of *Magnetosprillum magnetotacticum*) fall outside the central area of the diagram, no inorganically-produced population of magnetite crystals has yet been found which inhabits this central region. With the exception of particles in chains, elongated prismatic magnetite crystals in ALH84001 meet all other criteria and thus fall within the central region of this diagram.

inorganic growth mechanism that could produce particles with size distributions having sharp limits at these particular W/L ratios (Devouard et al., 1998). Conversely, the anisotropically grown (e.g., W/L ratio $\sim$ 0.7) magnetite crystals, such as those from MV-1, may be controlled by specific proteins located within the magnetosome membrane (Lowenstam, 1981; Mann and Frankel, 1986; Gorby et al., 1988). To date, elongated prismatic, single-domain magnetites with these axial ratios are not known to be produced by recognized terrestrial inorganic processes.

Additional criteria for distinguishing biogenic from abiotic magnetite might include unique isotopic signatures. Mandernack et al. (1999) recently showed that there was no detectable fractionation in Fe isotopes in magnetite produced intracellularly by magnetotactic bacterial strains MV-1 and *Magnetosprillum magnetotacticum.* In other recent work however, Beard et al. (1999) showed that dissimulatory Fe-reducing bacteria (e.g., *Shewanella alga*) potentially fractionate Fe isotopes during metal reduction. At this point it is unclear if this isotopic fractionation is reflected in the magnetite produced by these bacteria.

6. SUMMARY AND CONCLUSIONS

The magnetites in ALH84001 are demonstrably Martian in origin. We have described six specific properties of magnetite observed in magnetotactic bacteria that likely evolved through the process of natural (Darwinian) selection:

1. Single-domain size and restricted anisotropic W/L ratios.
2. Chemical purity.
3. Crystallographic perfection.
4. Crystals aligned in chains.
5. Unusual crystal morphology.
6. Crystallographic elongation along the [111] axis.

The magnetites that belong to the irregular and whisker populations of ALH84001 do not collectively display these

criteria. Accordingly, they cannot be considered biosignatures. Whether all or only some of the irregular and whisker magnetites formed within the carbonates, remains to be determined. While high temperature processes have been suggested for the whisker and/or irregular magnetites, this does not place constraints on the ALH84001 elongated prisms, which, we suggest, formed by processes similar to those that produce biogenic magnetite crystals on Earth.

The ALH84001 elongated prismatic magnetites display five of the six criteria required for their interpretation as a biosignature. The elongated prismatic magnetite crystals from ALH84001 carbonate globules are indistinguishable from biogenic magnetite particles produced by the strain of magnetotactic bacteria MV-1, suggesting similar mechanisms of formation.

Given the complexity of the ALH84001 meteorite, we believe that it would be simplistic to suggest that only a single mechanism explains all the observations related to the magnetite crystals within the carbonate globules. We note terrestrial samples of recent and ancient carbonates contain magnetite crystals of both inorganic and biogenic origin (Table A4). Many processes likely contributed to what is now observed, and *one* of these processes produced magnetite in the ALH84001 Martian meteorite that, in a terrestrial context, would be defined as biogenic.

Acknowledgments—We thank R.N. Zare, P. R. Buseck, H. Stanjek, R. B. Frankel, L. P. Keller, A. P. Taylor, and J. P. Bradley for constructive critical comments and the STI Center at Johnson Space Center, particularly J. Hultberg, for assistance. We thank B. Moskowitz, B. A. Hofmann, and an anonymous reviewer for greatly improving this manuscript. We also acknowledge the support of K. A. White, S. R. Keprta, M. F. McKay, The Honorable Tena Camp Bell, and D. C. Golden. We acknowledge the funding and support of NASA's Astrobiology and Exobiology Programs. DAB was also supported by United States National Science Foundation (NSF) grant CHE-9714101.

Special handling: C. Koeberl

REFERENCES

Abzalov M. Z. (1998) Chrome-spinels in gabbro-Wehrlite intrusions of the Pechenga area, Kola Peninsula, Russia: Emphasis on alteration features. *Lithos* **43,** 109–134.

Akai J., Iida A., Akai K., and Chiba A. (1997) Mn and Fe minerals of possible biogenic origin from two Precambrian stromatolites in western Australia. *J. Geol. Soc. Japan* **103,** 484–488.

Aumento F. and Mitchell W. S. (1975) Magnetic spherules from the mid-Atlantic ridge. *Geol.* **3,** 407–410.

Barber D. J. (1981) Matrix phyllosilicates and associated minerals in C2M carbonaceous chondrites. *Geochim. Cosmochim. Acta* **45,** 945–970.

Bazylinski D. A., Frankel R. B., and Jannasch H. W. (1988) Anaerobic magnetite production by a marine magnetotactic bacterium. *Nature* **334,** 518–519.

Bazylinski D. A. (1995) Structure and function of the bacterial magnetosome. *ASM News* **61,** 337–343.

Bazylinski D. A. and Moskowitz B. M. (1997) Microbial biomineralization of magnetic iron minerals: Microbiology, magnetism, and environmental significance. In *Geomicrobiology: Interactions between Microbes and Minerals* (eds. J. F. Banfield and K. H. Nealson). pp.181–223. Mineralogical Society of America, Washington, DC.

Beard B. L., Johnson C. M., Cox L., Sun H., Nealson K. H., and Aguilar C. (1999) Iron isotope biosignatures. *Science* **285,** 1889–1892.

Belkaaloul N. K. and Aissaoui D. M. (1997) Nature and origin of magnetic minerals within the Middle-Jurassic shallow-water carbonate rocks of the Paris Basin, France: Implications for magnetostratigraphic dating. *Geophys. J. Internat.* **130,** 411–421.

Belkaaloul K. N., Aissaoui D. M., Rebelle M., and Sambet G. (1997) Resolving sedimentological uncertainties using magnetostratigraphic correlation: An example from the Middle Jurassic of Burgundy, France. *J. Sediment. Res.* **67,** 676–685.

Benn K., Rochette J. L., and Hattori K. (1993) Magnetic susceptibility, magnetic mineralogy, and magnetic fabrics in a late Archean granitoid-gneiss belt. *Precamb. Res.* **63,** 59–81.

Bi D. and Morton R. D. (1995) Magnetic spherules from recent fluvial sediments in Alberta, Canada: Characteristics and possible origins. *Can. J. Earth Sci.* **32,** 351–358.

Blakemore R. P. (1975) Magneotactic bacteria. *Science* **190,** 377–379.

Borg L. E., Connelly J. N., Nyquist L. E., Shih C.-Y., Wisemann H., and Reese Y. (1999) The age of the carbonates in Martian meteorite ALH84001. *Science* **286,** 90–94.

Borradaile G. J., Chow N., and Werner T. (1993) Magnetic hysteresis of limestones: Facies control? *Phys. Earth Planet. Inter.* **76,** 241–252.

Borrok D. M., Kesler S. E., Boer R. H., and Essene E. J. (1998) The Vergenoeg magnetite-fluorite deposit, South Africa: Support for a hydrothermal model for massive iron oxide deposits. *Econ. Geol.* **93,** 564–586.

Bradley J. P., Harvey R. P., and McSween Jr. H. Y. (1996) Magnetite whiskers and platelets in the ALH84001 Martian meteorite; evidence of vapor phase growth. *Geochim. Cosmochim. Acta* **60,** 5149–5155.

Bradley J. P., McSween Jr. H. Y., and Harvey R. P. (1998) Epitaxial growth of nanophase magnetite in Martian meteorite Allan Hills 84001. *Meteor. Planet. Sci.* **33,** 765–773.

Braun V., Hantke K., and Koster W. (1998) Bacterial iron transport: Mechanisms, genetics, and regulation. *Metal Ions in Biological Systems* **35,** 67–145.

Butler R. F. and Banerjee S. K. (1975) Theoretical single-domain grain size range in magnetite and titanomagnetite. *J. Geophys. Res.* **80,** 4049–4058.

Campbell A. S., Schwertmann U., and Campbell P. A. (1997) Formation of cubic phases on heating ferrihydrite. *Clay Minerals* **32,** 615–622.

Chang S.-B. R., Kirschvink J. L., and Stolz J. F. (1987) Biogenic magnetite as a primary remanence carrier in limestone deposits. *Phys. Earth Planet. Int.* **46,** 289–303.

Chang S.-B. R. and Kirschvink J. L. (1989) Magnetofossils, the magnetization of sediments and the evolution of magnetite biomineralization. *Ann. Rev. Earth Planet. Sci.* **17,** 169–195.

Chang S.-B. R., Stolz J. F., Kirschvink J. L., and Awramik S. M. (1989) Biogenic magnetite in stromatolites II: Occurrence in ancient sedimentary environments. *Precamb. Res.* **43,** 305–315.

Cole D. R., Valley J. W., Spicuzza M. J., and Horita J. (1999) Oxygen-Isotopic fractionation between magnetite and water. *9th Annual V.M. Goldschmidt Conference*, LPI Contrib. #971, pp. 56. Lunar Planet. Inst., Houston. (abstr.).

Cornell R. M. and Schwertmann U. (1996) Crystal morphology and size. In *The Iron Oxides* pp. 53–86. VCH Press, Weinheim, Germany.

Dean A. J., and Bazylinski D. A. (1999) Genome analysis of several magnetotactic bacterial strains using pulsed-field gel electrophoresis. *Curr. Microbiol.* **39,** 219–225.

Devouard B., Posfai M., Hua X., Bazylinski D. A., Frankel R. B., and Buseck P. R. (1998) Magnetite from magnetotactic bacteria: Size distributions and twinning. *Am. Mineral.* **83,** 1387–1398.

Diaz-Ricci J. C. and Kirschvink J. L. (1992) Magnetic domain state and coercivity predictions for biogenic greigite (Fe_3S_4): Comparison of theory with magnetosome observations. *J. Geophys. Res.* **97,** 17 309–17,315.

Doukhan N., Ingrin J., Doukhan J. C., and Latrous K. (1990) Coprecipitation of magnetite and amphibole in black star diopside. *Am. Mineral.* **75,** 840–846.

Dunlop D. J., Schutts L. D., and Hale C. J. (1984) Paleomagnetism of Archean rocks from northwestern Ontario: III. Orck magnetism of the Shelly Lake granite, Quetico Subprovince. *Can. J. Earth Sci.* **21,** 879–886.

Eggleton R. A. and Boland J. N. (1982) Weathering of enstatite to talc

through a sequence of transitional phases. *Clays Clay Minerals* **30,** 11–20.
Einaudi M. T. and Burt D. M. (1982) Skarn deposits in the Yerington District, Nevada: Metasomatic skarn evolution near Ludwig. *Econ. Geol.* **77,** 877–898.
Elmore R. D., Engle M. H., Crawford L., Nick K., Imbus S., and Sofer Z. (1987) Evidence for a relationship between hydrocarbons and authigenic magnetite. *Nature* **325,** 428–430.
Elmore R. D. and Crawford L. (1990) Remanence in authigenic magnetite: Testing the hydrocarbon-magnetite hypothesis. *J. Geophys. Res.* **95,** 4539–4549.
Endress M. and Bischoff A. (1996) Carbonate in CI chondrites: Clues to parent body evolution. *Geochim. Cosmochim. Acta* **60,** 489–507.
Evans M. E. and McElhinny M. W. (1966) The paleomagnetism of the Modipe gabbro. *J. Geophys. Res.* **71,** 6053–6063.
Evans M. E. and McElhinny M. W. (1968) Single domain magnetite and high coercivities in a gabbroic intrusion. *Earth Planet. Sci. Lett.* **4,** 142–146.
Evans M. E. and Wayman M. L. (1970) An investigation of small magnetic particles by means of electron microscopy. *Earth Planet. Sci. Lett.* **9,** 365–370.
Farr M. R. and Gose W. A. (1991) Paleomagnetism of the Cambrian Moose Hollow Group, Texas: Evidence for a primary magnetization carried by detrital magnetite. *J. Geophys. Res.* **96,** 9895–9907.
Fassbinder J. W. E., Stanjek H., and Vali H. (1990) Occurrence of magnetic bacteria in soil. *Nature* **343,** 161–163.
Frankel R. B., Blakemore R. P., and Wolfe R. S. (1979) Magnetite in freshwater magnetotactic bacteria. *Science* **203,** 1355–1356.
Frankel R. B. and Blakemore R. P. (1980) Navigational compass in magnetic bacteria. *J. Magn. Magn. Mater.* **15,** 1562–1564
Frankel R. B., Bazylinski D. A., Johnson M. S., and Taylor B. L. (1997) Magneto-aerotaxis in marine coccoid bacteria. *Biophys. J.* **73,** 994–1000.
Frost R. B. (1991) Stability of oxide minerals in metamorphic rocks. In *Oxide Minerals: Petrologic and Magnetic Significance, Reviews in Mineralogy* **25,** 469–488. (ed. D. H. Lindsley). Bookcrafters, Inc., Chelsea, MI.
Frost R. B. and Lindsley D. H. (1991) Occurrence of iron-titanium oxides in igneous rocks. In *Oxide Minerals: Petrologic and Magnetic Significance, Reviews in Mineralogy* **25,** 433–468. (ed. D. H. Lindsley). Bookcrafters, Inc., Chelsea, MI.
Geissman J. W., Newberry N. G., and Peacor D. R. (1983) Discrete single-domain and pseudo-single-domain titanomagnetite particles in silicic glass of an ash-flow tuff. *Can. J. Earth Sci.* **20,** 334–338.
Geissman J. W., Harlan S. S., and Brearley A. J. (1988) The physical isolation and identification of carriers of geologically stable remanent magnetization: paleomagnetic and rock magnetic microanalysis and electron microscopy. *Geophys. Res. Lett.* **15,** 479–482.
Givargizov E. I. (1987) Highly Anisotropic Crystals. Terra Scientific Publishing, Tokyo.
Golden D. C., Ming D. W., Schwandt C. S., Morris R. V., Yang S. V., and Lofgren G. E. (1999) An experimetnal study of kinetically-driven precipitation of Ca-Mg-Fe carbonates from solution: Implications for the low-temperature formation of carbonates in Martian meteorite ALH84001. *Lunar Planet. Sci. XXX,* Lunar Planet. Inst., Houston #1973 (abstr.).
Golden D. C., Ming D. W., Schwandt C. S., Lauer H. V., Socki R. A., Morris R. V., Lofgren G. E., and McKay G. A. (2000) Inorganic formation of zoned Mg-Fe-Ca carbonate globules with magnetite and sulfide rims similar to those in Martian meteorite ALH84001. *Lunar Planet. Sci. XXXI,* Lunar Planet. Inst., Houston #1799 (abstr.).
Gooding J. L. (1992) Soil mineralogy and chemistry on Mars: Possible clues from salts and clays in SNC meteorites. *Icarus* **99,** 28–41.
Gorby Y. A., Beveridge T. J., and Blakemore R. P. (1988) Characterization of the bacterial magnetosome membrane. *J. Bacteriol.* **170,** 834–841.
Gorby Y. A. (1989) Regulation of magnetosome biogenesis by oxygen and nitrogen. Ph.D. thesis, Univ. New Hampshire.
Grigor'yev N. A., Sazonov V. N., Murzin V. V., and Gladkovsky B. A. (1990) Sulfides as gold carriers in skarn-magnetite deposit skarns and ores. *Geochem. Int.* **27,** 142–146.
Grigsby J. D. (1990) Detrital magnetite as a provenance indicator. *J. Sed. Pet.* **60,** 940–951.
Haese R. R., Petermann H., Dittert L., and Schulz H. D. (1998) The early diagenesis of iron in pelagic sediments: A multidisciplinary approach. *Earth Planet. Sci. Lett.* **157,** 233–248.
Hall D. L., Cohen L. H., and Schiffman P. (1988) Hydrothermal alteration associated with the Iron Hat iron skarn deposit eastern Mojave desert, San Bernardino County, California. *Econ. Geol.* **83,** 568–587.
Hall J. M. and Muzzatti A. (1999) Delayed magnetization of the deeper kilometer of oceanic crust at Ocean Drilling Project Site 504. *J. Geophys. Res.* **104,** 12,843–12,851.
Hargraves R. B. (1990) Magnetic properties, iron-titanium oxides, and petrology of four leg 115 basalts. In *Proc. Ocean Drilling Program, Scientific Results* **115,** 103–110.
Harvey R. P. and McSween Jr. H. Y. (1996) A possible high-temperature origin for the carbonates in the Martian meteorite ALH84001. *Nature* **382,** 49–51.
Heider F., Dunlop D. J., and Sugiura N. (1987) Magnetic properties of hydrothermally recrystallized magnetite crystals. *Science* **236,** 1287–1288.
Heider F., Lorner U., and Bitschene P. (1993) Volvanic ash particles as carriers of remnant magnetism in deep-sea sediments from Kerguelen Plateau. *Earth Planet. Sci. Lett.* **118,** 121–143.
Hesse P. P. (1994) Evidence for bacterial palaeoecological origin or mineral magnetic cycles in oxic and sub-oxic Tasman Sea sediments. *Mar. Geol.* **117,** 1–17.
Hoblitt R. P. and Larsen E. E. (1975) New combination of techniques for determination of ultrafine structure of magnetic minerals. *Geol.* **3,** 723–726.
Hounslow M. W. and Maher B. A. (1996) Quantitative extraction and analyses of carriers of magnetization in sediments. *Geophys. J. Int.* **124,** 57–74.
Hyman M. and Rowe M. W. (1983) Magnetite in CI chondrites. *J. Geophys. Res. Proc. 13th Lunar Planet. Sci. Conf., J. Geophys. Res.* **88**, Supplement (Part 2), A736–A740.
Ichinose N., Ozaki Y., and Kashu S. (1992) In *Superfine Particle Technology* (Chap. 1) pp. 11–17. Springer Verlag, London.
Ishikawa T., Kondo Y., Yasukawa A., and Kandori K. (1998) Formation of magnetite in the presence of ferric oxyhydroxides. *Corros. Sci.* **40,** 1239–1251.
Itoh Y., Katsura I., and Danhara T. (1989) Magnetic glasses in the Azuki and AT volcanic ashes in Japan. *Earth Planet. Sci. Lett.* **96,** 220–228.
Jackson M., McCabe C., Ballard M. M., and Van der Voo R. (1988) Magnetite authigenesis and diagenetic paleotemperatures across the northern Appalachian basin. *Geol.* **16,** 592–595.
Jedwab J. (1971) La magnetite de la meteorite d'Orgueil vue au microscope electronique a balayage. *Icarus* **15,** 319–340.
Jolivet J. P., Belleville P., Tronc E., and Livage J. (1992) Influence of Fe (II) on the formation of the spinel iron oxide in alkaline medium. *Clays Clay Mineral.* **38,** 196–202.
Joy D. C., Romig A. D., Goldstein J. I., eds. (1986) Principles of Analytical Electron Microscopy. Plenum Press, New York.
Jull A.J.T., Eastoe C.J., Xue S., Herzog G.F. (1995) Isotopic composition of carbonates in SNC meteorites Allan Hills 84001 and Nakhla. *Meteoritics* **30,** 311–318.
Kallemeyn G. W., Rubin A. E., and Wasson J. T. (1994) The compositional classification of chondrites: VI. The CR carbonaceous chondrite group. *Geochim. Cosmochim. Acta* **58,** 2873–2888.
Karlin R. and Levi S. (1984) Geochemical and sedimentological control of the magnetic properties of hemipelagic sediments. *J. Geophys. Res.* **90,** 10373–12336.
Karlin R. (1990) Magnetic mineral diagenesis in suboxic sediments at Bettis site W-N NE Pacific ocean. *J. Geophys. Res.* **95,** 4421–4436.
Keller K. P., Thomas K. L., and McKay D. S. (1992a) Thermal processing of cosmic dust: Atmospheric heating and parent body metamorphism. *Lunar Planet. Sci. XXIII,* Lunar Planet. Inst., Houston. pp. 675–676 (abstr.).
Keller L. P., Thomas K. L., and McKay D. S. (1992b) An interplanetary dust particle with links to CI chondrites. *Geochim. Cosmochim. Acta* **56,** 1409–1412.
Keller L. P., Thomas K. L., Clayton R. N., Makeda T. K., DeHart J. M., and McKay D. S. (1994) Aqueous alteration of the Bali CV3 chon-

drite: Evidence from mineralogy, mineral chemistry, and oxygen isotopic compositions. *Geochim. Cosmochim. Acta* **58,** 5589–5595.
Kerridge J. F. (1970) Some observations on the nature of the magnetite in the Orgueil meteorite. *Earth Planet. Sci. Lett.* **9,** 299–306.
Kerridge J. F., Mackay A. L., and Boynton W. V. (1979) Magnetite in CI carbonaceous meteorites; origin by aqueous activity on a planetesimal surface. *Science* **205,** 395–397.
Kilgore B. and Elmore R. D. (1989) A study of the relationship between hydrocarbon migration and the precipitation of authigenic magnetic minerals in the Triassic Chugwater formation, southern Montana. *Geol. Soc. Am. Bull.* **101,** 1280–1288.
Kirschvink J. L. (1980) South-seeking magnetic bacteria. *J. Exp. Biol.* **86,** 345–347.
Kirschvink J. L. and Lowenstam H. A. (1979) Mineralization and magnetization of chiton teeth: Paleomagnetic, sedimentilogic and biologic implications of organic magnetite. *Earth Planet. Sci. Lett.* **44,** 193–204.
Kirschvink J. L. (1982) Paleomagnetic evidence for fossil magnetite in western Crete. *Earth Planet. Sci. Lett.* **59,** 388–392.
Kirschvink J. L. (1983) Biogenic ferrimagnetism: A new biomagnetism. In *Biomagnetism: An Interdisciplinary Approach* (ed. S. Williamson) pp. 501–532. Plenum Press, New York.
Kirschvink J. L. and Chang S.-B. R. (1984) Ultrafine-grained magnetite in deep-sea sediments: Possible bacterial magnetofossils. *Geol.* **12,** 559–562.
Kirschvink J. L. (1992) On the magnetostatic control of crystal orientation and iron accumulation in magnetosomes. *Automedica* **14,** 257–269.
Krot A. N., Zolensky M. E., Wasson J. T., Scott E. R. D., Keil K., and Oshimi K. (1997) Carbide-magnetite assemblages in type-3 ordinary chondrites. *Geochim. Cosmochim. Acta* **61,** 219–237.
Larson M. S., Stone W. E., Morris W. A., and Crocket J. H. (1998) Magnetic signature of magnetite-enriched rocks hosting platinum-group element mineralization within the Archean Boston Creek Flow, Ontario. *Geophysics* **63,** 440–445.
Lawson C. A., Nord Jr. G. L., and Champion D. E. (1987) Fe-Ti oxide mineralogy and the origin of normal and reverse remanent magnetization in dacite pumice blocks from Mt. Shasta, California. *Physics Earth Planet. Int.* **46,** 270–288.
Lean C. M. B. and McCave I. N. (1998) Glacial to interglacial mineral magnetic and palæoceanographic changes at Chatham Rise, SW Pacific Ocean. *Earth Planet. Sci. Lett.* **163,** 247–260.
LeGuern F. and Bernard A. (1982) A new method for sampling and analyzing volcanic sublimates-application to Merapi volcano, Java. *J. Volcanology Geothermal Res.* **12,** 133–146.
Lovley D. R. (1991) Magnetite formation during microbial dissimilatory iron reduction. In *Iron Biominerals* (eds. R. B. Frankel and R. P. Blakemore) pp. 151–166. Plenum Press, New York.
Lovlie R., Lovlie W., and Jacobs J. (1971) Magnetic properties and mineralogy of four deep-sea cores. *Earth Planet. Sci. Lett.* **15,** 157–167.
Lowenstam H. A. (1981) Minerals formed by organisms. *Science* **211,** 1126–1131.
Lowther J. S. and Wisher A. P. (1996) Iron and titanium oxides in the rocks of Mt. Ranier volcano, Washington, state. *Geol. Soc. America, Abstracts with Program.* p. 86 (abstr.).
Lu G., Marshak S., and Kent D. V. (1990) Characteristics of magnetic carriers responsible for Late Paleozoic remagnetization in carbonates strata of the mid-continent, U.S.A. *Earth Planet. Sci. Lett.* **99,** 341–361.
Maher B. A. (1988) Magnetic properties of some synthetic sub-micron magnetites. *Geophys. J.* **94,** 83–96.
Maher B. A. and Taylor R. M. (1988) Formation of ultrafine-grained magnetite in soils. *Nature* **336,** 368–371.
Mandernack K. W., Bazylinski D. A., Shanks W. C., and Bullen T. D. (1999) Oxygen and iron isotope studies of magnetite produced by magnetotactic bacteria. *Science* **285,** 1892–1896.
Mann S., Frankel R. B., and Blakemore R. P. (1984a) Structure, morphology and crystal growth of bacterial magnetite. *Nature* **310,** 405–407.
Mann S., Moench T. T., and Williams R. J. P. (1984b) A high resolution electron microscopic investigation of bacterial magnetite: implications for crystal growth. *Proc. R. Soc. Lond. Ser. B* **221,** 385–393.
Mann S. (1985) Structure, morphology, and crystal growth of bacterial magnetite. In *Magnetite Biomineralization and Magnetoreception in Animals: A New Biomagnetism.* (eds. J. L. Kirschvink, D. S. Jones, B. J. McFadden) pp. 311–332. Plenum Press, New York.
Mann S. (1986) On the nature of boundary-organized biomineralization. *J. Inorg. Chem.* **28,** 363–371.
Mann S., Sparks N. H. C., and Blakemore R. P. (1987a) Structure, morphology and crystal growth of anisotropic magnetite crystals in magnetotactic bacteria. *Proc. R. Soc. Lond. Ser. B* **231,** 477–487.
Mann S., Sparks N. H. C., and Blakemore R. P. (1987b) Ultrastructure and characterization of anisotropic magnetic inclusions in magnetotactic bacteria. *Proc. R. Soc. Lond. Ser. B* **231,** 469–476.
Mann S., Sparks N. H. C., Walker M. M., and Kirschvink J. L. (1988) Ultrastructure, morphology, and organization of biogenic magnetite from sockeye salmon, *Oncorhynchus nerka*: Implications for magnetoreception. *J. Exp. Biol.* **140,** 35–49.
Mann S. and Frankel R. B. (1989) Magnetite biomineralization in unicellular organisms. In *Biomineralization: Chemical and Biochemical Perspectives* (eds. S. Mann, J. Web, R. J. P Williams) p. 426. VCH Press, Weinheim, Germany.
Mann S., Sparks N. H. C., Couling S. B., Larcomb M. C., and Frankel R. B. (1989) Crystallochemical characterization of magnetic spinels prepared from aqueous solution. *J. Chem. Soc. Faraday Trans.* **85,** 3033–3044.
Mann S., Sparks N. H. C., and Wade V. J. (1991) Crystallochemical control of iron oxide biomineralization. In *Iron Biominerals* (eds. R. B. Frankel and R. P. Blakemore) p. 435. Plenum Press, New York.
Matthews A. (1976) Magnetite formation by the reduction of hematite with iron under hydrothermal conditions. *Am. Mineral.* **61,** 927–932.
McCabe C., Sassen R., and Saffer B. (1987) Occurrence of secondary magnetite within biodegraded oil. *Geol.* **15,** 7–10.
McCabe C., Van der Voo R., Peacor D. R., Scotese C. R., and Freeman R. (1983) Diagenetic magnetite carries ancient yet secondary remnance in some Paleozoic sedimentary carbonates. *Geol.* **11,** 221–223.
McClay (1974) Single-domain magnetite in the Jimberlana norite, western Australia. *Earth Planet. Sci. Lett.* **21f,** 367–376.
McKay D. S., Gibson E. K. Jr., Thomas-Keprta K. L., Vali H., Romanek C. S., Clemett S. J., Chillier X. D. F., Maechling C. R., and Zare R. N. (1996) Search for past life on Mars: Possible relic biogenic activity in Martian meteorite ALH84001. *Science* **273,** 924–930.
McNeill D. F. (1990) Biogenic magnetite from surface Holocene carbonate sediments, Great Bahama Bank. *J. Geophys. Res.* **95,** 4363–4371.
McNeill D. F. (1993) A review and comparison of carbonate rock magnetization: Leg 133, Queensland Plateau, Australia. *Proc. Ocean Drilling Program, Scientific Results* **133,** 749–753
McNeill D. F. and Kirschvink J. L. (1993) Early dolomitization platform carbonates and the preservation of magnetic polarity. *J. Geophys. Res.* **98,** 7977–7986.
McNeill D. F., Ginsberg R. N., Chang S.-B. R., and Kirschvink J. L. (1988) Magnetostratigraphic dating of shallow-water carbonates from San Salvador, Bahamas. *Geol.* **16,** 8–12.
McNeill D. F., Guyomard T. S., and Hawthorne T. B. (1993) Magnetostratigraphy and the nature of magnetic remanence in platform/periplatform carbonates, Queensland Plateau, Australia. *Proc. Ocean Drilling Program, Scientific Results* **133,** 573–587.
McSween H. Y. Jr. and Harvey R. P. (1998) An evaporation model for formation of carbonates in the ALH84001 Martian meteorite. *Int. Geology Review* **40,** 774–783.
Meldrum F. C., Mann S., Heywood B. A., Frankel R. B., and Bazylinski D. A. (1993a) Electron microscope study of magnetosomes in a cultured coccoid magnetotactic bacterium. *Proc. R. Soc. Lond. Ser. B* **251,** 231–236.
Meldrum F. C., Mann S., Heywood B. R., Frankel R. B., and Bazylinski D. A. (1993b) Electron microscopy study of magnetosomes in two cultured vibrioid magnetotactic bacteria. *Proc. R. Soc. Lond. Ser. B* **251,** 237–242.
Michel, S. H. and Pasteris, J. D. (1981) The petrologic relationships

between magnetite and hematite in the Pilot Knob iron deposit, southeastern, Missouri. *Geol. Soc. America* **13,** 510 (abstr.).
Mittlefehldt D. W. (1994) ALH84001, a cumulate orthopyroxenite member of the Martian meteorite clan. *Meteoritics* **29,** 214–221.
Modreski, P. J. and Chou, I.-M. (1981) The silica content of magnetite form the fayalite-magnetite-quartz assemblage and from hydrothermal ore deposits. *Geol. Soc. America Bull.* **13,** 513 (abstr.).
Moecher D. P., Anderson E. D., Cook C. A., and Mezger K. (1997) The petrogenesis of metamorphosed carbonates in the Grenville Province, Ontario. *Can. J. Earth Sci.* **34,** 1185–1201.
Montgomery P., Hailwood E. A., Gale A. S., and Burnett J. A. (1998) The magnetostratigraphy of Coniacian-Late Campanian chalk sequences in southern England. *Earth Planet. Sci. Lett.* **156,** 351–361.
Morgan G. E. and Smith P. P. K. (1981) Transmission electron microscope and rock magnetic investigations of remanence carriers in a Precambrian metadolerite. *Earth Planet. Sci. Lett.* **53,** 226–240.
Morris R. V., Golden D. C., Bell J. F., Lauer H. V., and Adams J. B. (1993) Pigmenting agents in Martian soils: Inferences from spectral, Mossbauer and magnetic properties of nanophase and other iron oxides in Hawaiian palagonitic soil PN-9. *Geochim. Cosmochim. Acta* **57,** 4597–4609.
Moskowitz B. M., Frankel R. B., Bazylinski D. A., Jannasch H. W., and Lovley D. R. (1989) A comparison of magnetite particles produced anaerobically by magnetotactic and dissimilatory iron-reducing bacteria. *Geophys. Res. Lett.* **16,** 665–668.
Nicholls D. (1987) Complexes and First-Row Transition Elements, Macmillan Education, Ltd., London. pp. 172–183.
Nyquist L. E., Bansal B. M., Wiesmann H., Shih C.-Y. (1995) "Martians" young and old: Zagami and ALH84001. *Lunar Planet. Sci. XXVI,* Lunar Planet. Inst., Houston. p. 1065 (abstr.).
Nystrom J. O. and Hendriquez F. (1994) Magmatic features of iron ores of the Kiruna type in Chile and Sweden: Ore textures and magnetite geochemistry. *Econ. Geol.* **89,** 820–839.
Otten M. T. (1985) The subsolidus history of the Artfallet gabbro: A TEM study of olivine, sugite, and orthopyroxene. *J. Pet.* **26,** 488–514.
Paoletti L. C. and Blakemore R. P. (1986) Hydroxamate production by *Aquaspirillum magnetotacticum. J. Bacteriol.* **167,** 73–76.
Peck J. A. and King J. W. (1996) Magnetofossils in the sediment of Lake Baikal, Siberia. *Earth Planet. Sci. Lett.* **140,** 159–172.
Perkins A. M. (1996) Observations under electron microscopy of magnetite minerals extracted from speleothems. *Earth Planet. Sci. Lett.* **139,** 281–289.
Petersen N., von Dobenek T., and Vali H. (1986) Fossil bacterial magnetite in deep-sea sediments from the south Atlantic ocean. *Nature* **320,** 611–615.
Pick T. and Tauxe L. (1994) Characteristics of magnetite in submarine basaltic glass. *Geophys. J. Int.* **119,** 116–128.
Pucher R. (1969) Relative stability of chemical and thermal remanence in synthetic ferrites. *Earth Planet. Sci. Lett.* **6,** 107–111.
Pullar R. C., Pyke D. R., Taylor M. D., and Bhattacharya A. K. (1998) The manufacture and characterization of single phase magnetite and hematite aligned fibres from an aqueous sol-gel process. *J. Mat. Sci.* **33,** 5229–5235.
Razjigaeva N. G. and Naumova V. V. (1992) Trace element composition of detrital magnetite from coastal sediments of northwestern Japan sea for provenance study. *J. Sed. Pet.* **62,** 802–809.
Rhodes A. L., Oreskes N., and Sheets S. (1997) Recognition of a paleo-hydrothermal system responsible for magnetite formation at El Laco, Chile. *Trans. Am. Geophys. Union, EOS Supp.* **46,** 748–749 (abstr.).
Romanek C. S., Grady M. M., Wright I. P., Mittlefehldt D. W., Socki R. A., Pillinger C. T., and Gibson E. K. Jr. (1994) Record of fluid-rock interactions on Mars from the meteorite ALH84001. *Nature* **372,** 655–657.
Rubin A. E. (1993) Magnetite-sulfide chondrules and nodules in CK carbonaceous chondrites: Implications for the timing of CK oxidation. *Meteoritics* **28,** 130–135.
Saffer B. and McCabe C. (1992) Further studies of carbonate remagnetization in the northern Appalachian basin. *J. Geophys. Res.* **97,** 4331–4348.
Schlinger C. M. and Smith R. M. (1986) Superparamagnetism in volcanic glasses of the KBS Tuff: Transmission electron microscope and magnetic behavior. *Geophys. Res. Lett.* **13,** 729–732.
Schlinger C. M., Grisom G. C., Papaefthymiou G. C., and Veblen D. R. (1988) The nature of magnetic single domains in volcanic glasses of the KBS Tuff. *J. Geophys. Res.* **93,** 9137–9156.
Schoen M. and Diestler D. J. (1987) Epitaxy in simple fluids in micropores and near solid surfaces. *Geol. Soc. America* **66,** 1281 (abstr.).
Schwartz M., Lund S. P., Hammond D. E., Schwartz R., and Wong K. (1997) Early sediment diagenesis on the Blake/Bahama outer ridge, North Atlantic ocean and its effects on sediment magnetism. *J. Geophys. Res.* **102,** 7903–7914.
Schwertmann U. and Murad E. (1990) The influence of aluminum on iron oxides: XIV. Aluminum substituted magnetite synthesized at ambient temperatures. *Clays Clay Mineral.* **38,** 196–202.
Schwertmann U. and Cornell R. M. (1991) Magnetite. In *Iron Oxides in the Laboratory; Preparation and Characterization.* VCH Press, Weinheim, Germany, 137 pp.
Scott E. R. D., Krot A. N., and Yamaguchi A. (1998) Carbonates in fractures of Martian meteorite ALH 84001: Petrologic evidence for impact origin. *Meteorit. Planet. Sci.* **33,** 709–719.
Shau Y. H., Peacor D. R., and Essene E. J. (1993) Formation of magnetic single domain magnetite in ocean ridge basalts with implications for sea-floor magnetism. *Science* **261,** 34–36.
Shihui Y. (1982) An approach to the genesis of magnetite deposit, Yinachang, Yunnan, from the internal structures of magnetite. *Bull. Chengdu Inst. Geology, Chinese Acad. Geol. Sci.* **3,** 137–147.
Sidhu P. S., Gilkes R. J., and Posner A. M. (1980) The behavior of Co, Ni, Zn, Cu, Mn, and Cr in magnetite during alteration to maghemite and hematite. *Soil Sci. America J.* **44,** 135–138.
Sitzman S.D., Banfield J.F. and Valley J.W. (2000) Microstructural characterization of two metamorphic magnetites with implications for oxygen isotope distribution. *Am. Mineral.* **85,** 14–21.
Smith P. P. K. (1979) The identification of single-domain titanomagnetite particles by means of transmission electron microscopy. *Can. J. Earth Sci.* **16,** 375–379.
Snowball I. F. (1994) Bacterial magnetite and the magnetic properties of sediments in a Swedish lake. *Earth Planet. Sci. Lett.* **126,** 129–142.
Sparks N. C. H., Mann S., Bazylinski D. A., Lovley D. R., Jannasch H. W., and Frankel R. B. (1990) Structure and morphology of magnetite anaerobically-produced by a marine magnetotactic bacterium and dissimilatory iron-reducing bacterium. *Earth Planet. Sci. Lett.* **98,** 14–22.
Stenina N. G., Mazurov M. P., and Titov A. T. (1979) Mechanism of magnetite deposition in calcareous skarn. *Trans. (Doklady) U.S.S.R. Acad. Sciences, Earth Science Sec.* **249,** 694–698.
Stolper E. and McSween H. Y. Jr. (1979) Petrology and origin of the shergottite meteorites. *Geochim. Cosmochim. Acta* **43,** 1475–1498.
Stolz J. F., Chang S.-B. R., and Kirschvink J. L. (1986) Magnetotactic bacteria and single-domain magnetite in hemipelagic sediments. *Nature* **321,** 849–851.
Stolz J. F., Chang S.-B. R., and Kirschvink J. L. (1989) Biogenic magnetite in stromatolites: I. Occurrence in modern sedimentary environments. *Precam. Res.* **43,** 295–304.
Stolz J. F., Lovley D. R., and Haggerty S. E. (1990) Biogenic magnetite and the magnetization of sediments. *J. Geophys. Res.* **95,** 4355–4361.
Suk D., Peacor D. R., and Van der Voo R. (1990a) Replacement of pyrite framboids by magnetite in limestone and implications for paleomagnetism. *Nature* **345,** 611–613.
Suk D., Van der Voo R., and Peacor D. R. (1990b) Scanning and transmission electron microscope observations of magnetite and other iron phases in Ordovician carbonates from east Tennessee. *J. Geophys. Res.* **95,** 12,327–12,336.
Suk D., Van der Voo R., and Peacor D. R. (1991) SEM/TEM observations of magnetite in carbonates of eastern north America: Evidence for chemical remagnetization during the Alleghenian orogeny. *Geophys. Rev. Lett.* **18,** 939–942.
Suk D., Van der Voo R., and Peacor D. R. (1992) SEM/TEM observation of magnetic minerals in presumably unremagnetized Paleozoic carbonate from Indiana and Alabama. *Tectonophysics* **215,** 255–272.

Suk D., Van der Voo R., and Peacor D. R. (1993a) Origin of magnetite responsible for remagnetism of early Paleozoic limestones of New York state. *J. Geophys. Res.* **98,** 419–434.

Suk D., Van der Voo R., Peacor D. R., and Lohmann K. C. (1993b) Late Paleozoic remagnetization and its carrier in the Trenton and Black River carbonates from the Michigan basin. *J. Geol.* **101,** 795–808.

Sun W. and Jackson M. (1994) Scanning electron microscopy and rock magnetic studies of magnetic carrers in remagnetized early Proterozoic carbonates from Missouri. *J. Geophys. Res.* **99,** 2935–2942.

Symonds R. B., Rose W. I., Reed M. H., Lichte F. E., and Finnegan D. L. (1987) Volatilization, transport and sublimation of metallic and non-metallic elements in high temperature gases at Merapi Volcano, Indonesia. *Geochim. Cosmochim. Acta* **51,** 2083–2101.

Symonds R. (1993) Scanning electron microscope observations of sublimates from Merapi Volcano, Indonesia. *Geochem. J.* **26,** 337–350.

Taylor R. M. (1981) Non-silicate oxides and hydroxides. In *Chemistry of Clays and Clay Minerals* (ed. A. C. D. Newman). pp. 129–201. Wiley-InterScience, New York.

Thomas-Keprta K. L., Bazylinski D. A., Golden D. C., Wentworth S. J., Gibson E. K. Jr., and McKay D. S. (1998) Magnetite from ALH84001 carbonate globules: Evidence of biogenic signatures. *Lunar Planet. Sci. XXIX***,** Lunar Planet. Inst., Houston. #1494 (abstr.).

Thomas-Keprta K. L., Wentworth S. J., McKay D. S., Bazylinski D. A., Bell M. S., Romanek C. S., Golden D. C., and Gibson E. K. Jr. (1999) On the origins of magnetite in Martian meteorite ALH84001. *Lunar Planet. Sci. XXX***,** Lunar Planet. Inst., Houston. #1856 (abstr.).

Tople-Schadt J. and Muller W. F. (1985) The submicroscopic structure of the unequilibrated ordinary chondrites Chainpur, Mezo-Madaras and Tieschitz: A transmission electron microscope study. *Earth Planet. Sci. Lett.* **74,** 1–12.

Towe K. M. and Moench T. T. (1981) Electron-optical characterization of bacterial magnetite. *Earth Planet. Sci. Lett.* **52,** 213–220.

Treiman A. (1998) The history of ALH84001 revised: Multiple shock events. *Meteor. Planet. Sci.* **33,** 753–764.

Treiman A. H. and Romanek C. S. (1998) Bulk and stable isotopic compositions of carbonate minerals in Martian meteorite ALH84001: No proof of high temperature formation. *Meteor. Planet. Sci.* **33,** 737–742.

Ueno H. (1986) Chemical composition of magnetite from the hydrothermal alteration zone of quartz diorite bodies, Chichibu mining area, Japan. *Rock Magnetism and Paleogeophysics* **13,** 60–65.

Valdespino O. E. M. and Alvarez V. C. (1997) Paleomagnetic and rock magnetic evidence for inverse zoning in the Parguaza batholith (southwestern Venezuela) and its implications about tectonics of the Guyana shield. *Precam. Res.* **85,** 1–25.

Vali H., Forster O., Amarantidid G., and Petersen N. (1987) Magnetotactic bacteria and their magnetofossils in sediments. *Earth Planet. Sci. Lett.* **86,** 389–400.

Vali H. and Kirschvink J. L. (1989) Magnetofossil dissolution in a paleomagnetically unstable deep-sea sediment. *Nature* **339,** 203–206.

Vali H., von Dobeneck T., Amarantidis G., Forster O., Morteani G., Bachmann L., and Petersen N. (1989) Biogenic and lithogenic magnetic minerals in Atlantic and Pacific deep sea sediments and their paleomagnetic significance. *Geol. Rundschau* **78,** 753–764.

Vali H. and Kirschvink J. L. (1991) Observation of magnetosome organization surface structure and iron biomineralization of undescribed magnetic bacteria: Evolutionary speculations. In *Iron Biominerals* (eds. R. B. Frankel and R. P. Blakemore) 97–115. Plenum Press, New York.

Valley J. W., Eiler J. M., Graham C. M., Gibson E. K., Romanek C. S., and Stolper E. M. (1997) Low-temperature carbonate concretions in the Martian meteorite ALH84001: Evidence from stable isotopes and mineralogy. *Science* **275,** 1633–1638.

Van der Hoeven K. J., Knauth L. P., and Burt D. M. (1999) Extremely low temperature magnesian skarns: Chrysotile deposits of the Salt River Canyon area, central Arizona. *Geol. Soc. America,* A-161 (abstr.).

Van der Voo R., Fang W., Wang Z., Suk D., Peacor D. R., and Liang Q. (1993) Paleomagnetism and electron microscopy of the Emeishan basalts, Yunnan, China. *Tectonophysics* **221,** 367–379.

Vayssieres L., Chaneac C., Tronc E., and Jolivet J. P. (1998) Size tailoring of magnetite particles formed by aqueous precipitation: An example of thermodynamic stability of nanometric oxide particles. *J. Colloid Interface Sci.* **205,** 205–212.

Veizer J. (1983) Trace elements and isotopes in sedimentary carbonates. In *Rev. Mineral.; Carb.: min. and chem.,* **11,** 265–299. (ed. R. J. Reeder), Bookcrafters, Chelsa, MI.

Vidal C. C. E., Injoque-Esinoza J., Sidder G. B., and Mukasa S. B. (1990) Amphibolitic Cu-Fe skarn deposits in the central coast of Peru. *Econ. Geol.* **83,** 1447–1461.

Visalakshi G., Venkateswaran G., Kulshreshtha S. K., and Moorthy P. N. (1993) Compositional characteristics of magnetite synthesized from aqueous solution at temperatures up to 523 K. *Mat. Resource Bull.* **28,** 829–836.

Wang Z. and Van der Voo R. (1993) Rapid apparent polar wandering of South China during the latest Paleozoic and early Mesozoic: A paleomagnetic study of Upper Permian limestones from Guizhou province. *Tectonophysics* **222,** 165–176.

Wang G., Whitaker G., Harrison A., and Song L. (1998) Preparation and mechanism of formation of acicular goethite-magnetite particles by decomposition of ferric and ferrous salts in aqueous solution using microwave radiation. *Mat. Resource Bull.* **33,** 1571–1579.

Warren P. H. (1998) Petrologic evidence for low-temperature, possibly flood-evaporitic origin of carbonates in the ALH84001 meteorite. *J. Geophys. Res.* **103,** 16 759.

Worm H.-U. and Markert H. (1987) The preparation of dispersed titanomagnetite particles by the glass-ceramic method. *Phys. Earth Planet. Int.* **46,** 263–269.

Xu W., Van der Voo R., and Peacor D. R. (1994) Are magnetite spherules capable of carrying stable magnetizations? *Geophys. Res. Lett.* **21,** 517–520.

Xu W., Van der Voo R., Peacor D.R., and Beauboeuf R.T. (1997) Alteration and dissolution of fine-grained magnetite and its effects on magnetization of the ocean floor. *Earth Planet. Sci. Lett.* **151,** 279–288.

Xu W., Van der Voo R., and Peacor D. R. (1998) Electron microscopic and rock magnetic study of remagnetized Leadville carbonates, central Colorado. *Tectonophysics* **296,** 333–362.

Yitai Q., Yi X., Chuan H., Jing L., and Zuyao C. (1994) Hydrothermal preparation and characterization of ultrafine magnetite powders. *Mat. Res. Bull.* **29,** 953–957.

Zhang C., Vali H., Romanek C. S., Phelps T. J., and Lu S. V. (1998) Formation of single domain magnetite by thermophilic bacterium. *Am. Mineral.* **61,** 927–932.

Table A1. Sizes and axial ratios of magnetite (Fe_3O_4) particles in ALH84001 terrestrial magnetotactic bacteria, and selected inorganic and extracellular biogenic samples.

Magnetite morphology	Number of crystals	Length (nm) min-max	Length (nm) mean	Width (nm) min-max	Width (nm) mean	Width/length ratio	Width/length range
ALH84001 elongated prisms (this work)	164	18–89	39 (±15.5)	11–71	27 (±11.0)	0.7 (±0.09)	0.4–0.9
ALH84001 whiskers (this work)	41	6–625	76 (±117.8)	1–64	11 (±11.8)	0.2 (±0.08)	0.1–0.3
ALH84001 irregular (this work)	389	7–154	33 (±25.2)	7–109	26 (±18.5)	0.8 (±0.15)	0.3–1.0
Magnetotactic bacterial strain MV-1 (this work)	206	6–69	42 (±13.0)	6–46	30 (±8.5)	0.7 (±0.1)	0.5–1.0
Elongated prismatic magnetite (magnetotactic bacterial strain MV-1) (Sparks et al., 1990)	89	21–74	53	12–54	35	0.7	—
MV-2 (Meldrum et al., 1993b)	>200	30–59	48 ± 5	28–40	26 ± 7	0.6	—
MC-1[a] (Meldrum et al., 1993a)	~600	30–110	83 ± 14	15–107	78 ± 11	0.8	—
Commercially produced (this work)	85	5–100	32 ± 21	5–90	32 ± 21	1.0	—
Precipitated from aqueous solution (Schwertmann and Cornell, 1991)		50–200		50–200		~1.0	—
Extracellularly produced magnetite (Zhang et al., 1998)			56 ± 25		56 ± 25	~1.0	—

[a] Based on sizes of magnetite in cells grown in acetate-based media.

Table A2. Terrestrial inorganic magnetite in igneous (I) or metamorphic (M) rocks.

Rock type	Morphology	Size	Chemical composition	References
I/M	Wide variety	<1 μm to mm in size	Generally + Ti ($Fe_{3-x}TixO_4$; $0 \leq x \leq 0.8$) Fe commonly substituted by Ti, Mg, Mn, Ni, Zn, Al, Cr, and V	(Cornell and Schwertman, 1996; Frost, 1991; Frost and Lindsley, 1991) Enormous amount of literature on magnetic phases in the field of paleomagnetism summarized
I (carbonatites)	Irregular	1 mm longest direction		(Moecher et al., 1997)
I	Rods and plates	<17 μm		(Evans and McElhinny, 1968; Evans and McElhinny, 1966)
I	Irregular/equant	30 nm-2 μm; most multi-domain		(Evans and Wayman, 1970)
I	Equant/elongated	10–500 nm	+Ti	(Morgan and Smith, 1981)
I		100–200 μm (0.5 mm max)	<1 wt% TiO_2, trace V (magnetite/ilmenite intergrowth)	(Morgan and Smith, 1981)
I	Some needles	200–400 nm wide, 2.4 μm long		(Morgan and Smith, 1981)
I (in glass)	Irregular, hexagonal	Single-domain to pseudosingle-domain; <1 μm to μm-sized	+Ti	(Heider et al., 1993)
I (in glass)	Spheres	10–20 nm	+Ti	(Pick and Tauxe, 1994)
I (in glass)	Rounded	1.5–10 nm		(Schlinger et al., 1988)
I (in glass)		~10 nm		(Schlinger and Smith, 1986)
I (in glass)	Rounded, irregular	Single-domain	+Ti	(Itoh et al., 1989)
I	Crystalline aggregates and small isolated crystals	15–20 μm; 5–10 μm	+Ti, Mn	(LeGuern and Bernard, 1982)
I (in glass)	Irregular/hexagonal	Small as 40 nm	+Ti	(Smith, 1979)
I (in glass)		Pseudosingle- and single-domain	+Ti	(Geissman et al., 1983)
I	Octahedrons/elongated	Up to 50 μm	+Al, Ti	(Symonds et al., 1987; Symonds, 1993)
M	Microstructures in magnetite: Dislocations and channels filled with layer silicates; microvugs, spinel platelets		+ Variable Al (notable differences in exsolution behavior based on Al content)	(Sitzman et al., 2000)
I	Subhedral/euhedral	Typically few hundred μm	+Ti	(Shau et al., 1993)

(Continued)

Table A2. (Continued)

Rock type	Morphology	Size	Chemical composition	References
M	Platelet/needles in diopside	~200 nm–350 μm		(Doukhan et al., 1990)
I	Dentritic/irregular	Typically few hundred μm	+Ti	(Hargraves, 1990)
I	a. Euhedral/ subhedral b. Anhedral c. Irregular	a. 1–50 μm b. <20 μm c. <1 μm	All essentially pure; <0.3 oxide % Ti, Cr, Mn, V	(Benn et al., 1993)
I	Octrahedra; dendritic, columnar/platy	Up to hundreds of mm in size	+V, Ti, Al, Mg, Mn, Ni, Co, Zn, Cu, and Cr	(Nystrom and Hendriquez, 1994)
I/M	Euhedral/elongated/ acicular needles	<300 nm; 1–2 μm	+Ti (esp. larger grains)	(Geissman et al., 1988)
I (in glass)	Irregular	100–200 μm; <10 μm	+Ti; smaller Ti free	(Lawson et al., 1987)
I	Spheroids/equant	Smallest ~ 50 nm		(Hoblitt and Larsen, 1975)
i (in glass)	Dendritic/cruciform/ irregular	Pseudosingle-domain to multi-domain (1–10 μm)	+Ti	(Xu et al., 1997)
I	Irregular		+Ti	(Larson et al., 1998)
I		<0.2–30 μm	+Ti	(McClay, 1974)
I			+Ti (typical)	(Lowther and Wisher, 1996)
I/detrital (17 deep sea cores)	3 types: rounded/ angular/ octahedral	40% < 1 μm; most <8μm		(Lovlie et al., 1971)
I/M in sediments			11 trace elements detected: +Ti, Mn, Cr, V, Ni, Co, Zr, Sn, Zn, Pb, Cu	(Razjigaeva and Naumova, 1992)
I/M	Polymineralic, monomineralic	Differentiation of volcanic/metamorphic from detrital	+Ti, Mg, V, Al	(Grigsby, 1990, and references therein)
I/M	Cubic, very elongated plates, dendritic	1–100 μm		(Otten, 1985)
I	Irregular	Superparamagnetic, single-domain, multi-domain	Pure +Ti (Ti-magnetite)	(Valdespino and Alvarez, 1997)
I	Irregular	Three size rnages: 50–500 μm; 1–5 μm; <1 μm	Pure magnetite; some lamellae are hematite	(Dunlop et al., 1984)
I		20 nm up to 1000 μm	+Ti, Si, Al, Mg	(Morris et al., 1993)

Table A3. Terrestrial hydrothermally produced magnetites.

Rock type	Morphology	Size	Chemical composition/ interpretation	References
Andesitic volcanic rocks	Layers/octahedra	Coarse-grained	Metasomatic replacement of andesite and hydrothermal alteration (250–350°C)	(Rhodes et al., 1997)
Massive Fe-oxide deposit	a. Rimming ilmenite b. Radiating clusters of euhedral crystals c. Spherical to elongated droplets in fluorite	a. Tens of μm c. <100 nm	>1 wt% Ti hydrothermal fluids of magmatic origin	(Borrok et al., 1998)
Basalts	a. Cruciform/dendritic b. Anhedral/subhedral	a. Up to tens of μm b. >1 μm	a. +Ti to pure b. Pure anhedral/subhedral alteration products of primary igneous (dendritic)	(Van der Voo et al., 1993)
Fe-skarm	Irregular	mm in size	+Ti	(Vidal C. et al., 1990)
Skarns			+Al, Ca, Mg	(Grigor'yev et al., 1990)
Greenschist facies	Rims of magnetite on ilmenite/spinels and veinlets cross-cutting Cr-spinels		+Ti magmatic and hydrothermal alteration (serpentinization of olivine)	(Abzalov, 1998)
Ocean crust	Lamellae replacement	Many μm	+Ti fine-grained exsolution of TiO_2 from magnetite and hydrothermal (100–300°C) dissolution and redeposition of magnetite on surfaces of ilmenite lamellae	(Hall and Muzzatti, 1999)

(Continued)

Table A3. (Continued)

Rock type	Morphology	Size	Chemical composition/ interpretation	References
Quartz diorite	a. Euhedral/subhedral b. Aggregates/subhedral c. Fine-grained	a. 150 μm or less b. 10 μm	+Al, V, Cr, Mn, Mg aggregates and fine-grained recrystallized with lower amounts of listed elements	(Ueno, 1986)
Copper-bearing magnetite deposit	Round, laths, short prisms, elongated strips, irregular	2–3 μm	+Si, Al, Mg, Cl, K	(Shihui, 1982)
Calcareous skarn	a. Coarse-grained/ euhedral b. Faceted microcrystalline c. Identically oriented, single and polycrystalline aggregates (defect rich)	b. <100 nm c. <several hundred μm	Magnetite from reaction of hydrothermal solution with pyroxene, etc.	(Stenina et al., 1979)
Skarns	Bladed/prismatic		+Ma, Ca formation from hematite	(Einaudi and Burt, 1982)
Fe-skarn			Fluid inclusions (contain Ca-, Na-, K-chlorides) in magnetite suggest precipitation from solution (min T = 375°C)	(Hall et al., 1988)
Magnesian skarn	Extremely fine-grained		200–250°C hydrothermal alteration of limestone	(Van der Hoeven et al., 1999)
Skarns and fayalite/ magnetite/quartz assemblage			+Si, inclusion free	(Modreski and Chou, 1981)
Fe deposit	a. Coarse-grained and euhedral b. Fine-grained		a. From magma b. Replaces hematite	(Michel and Pasteris, 1981)

Table A4. Magnetite in low-temperature environments.

Rock type	Morphology	Size	Chemical composition Interpretation	References
Deep sea sediments	a. Elongated prismatic, bullet, octahedra b. Euhedral, with ilmenite exsolution lamellae	a. Single-domain (30–100 nm) b. Coarse	a. Biogenic b. +Ti, Mg, Al, Mn, Cr/pure compositions scarce	(Petersen et al., 1986)
Speleothem	a. Irregular/ equidimensional b. Hexagonal/cubic outlines	a. 0.01 to >10 μm b. 10–100 nm	a. Some +Ti b. Some biogenic	(Perkins, 1996)
Soils	Octagonal/hexagonal outlines	<10–100 nm	+Zn, Mn occasionally	(Maher and Taylor, 1988)
Carbonate		a. Single-domain b. Multi-domain c. Spheres c. >10 μm	a. Biogenic b. +Ti	(Belkaaloul et al., 1997)
Carbonate	a. Botryoidal/sphere aggregates b. Spheres	a. 3–20 μm b. Up to 150 μm	b. Inclusions: +Mg, Al, Si, Ca	(McCabe et al., 1983)
Carbonate	a. Spheres/dimpled surfaces b. Nonspherical/ c. Void filling	a. 1–35 μm b. Submicron to 50 μm		(Suk et al., 1990b)
Lake sediments	Prismatic	Single-domain	Biogenic	(Snowball, 1994)
Carbonate	Hollow spheroids; botryoidal			(Jackson et al., 1988)
Limestones	a. Spherical pseudoframboids b. Irregular/octahedral c. Aggregates of rounded grains	a. Up to 15 μm b. 1–10 μm c. ~200 nm		(Suk et al., 1993a)

(Continued)

Table A4. (Continued)

Rock type	Morphology	Size	Chemical composition/ interpretation	References
Carbonate	Slightly rounded, equant	80 μm max	+Ti	(Farr and Gose, 1991)
Carbonates	Spherical, botryoidal, nonspherical	μm-sized	Crystallized from fluid	(Suk et al., 1991)
Carbonates	a. Spherical and euhedral b. Framboids and spheres; irregular	a. 0.2–1 μm b. 10–20 μm		(Sun and Jackson, 1994)
Carbonaceous sediments	Subhedral to euhedral	$<$2 μm; 5–50 μm		(Karlin and Levi, 1984)
Suboxic sediments	Euhedral, roughly equidimensional	60–120 min; μm-sized	1.5 μ, +Ti $<$ 0.5 μm, pure	(Karlin, 1990)
Limestone	a. Spheres b. Octahedral or cubooctahedral	a. μm-sized b. $<$1 μm		(Suk et al., 1990a)
Limestones		a. Single-domain b. Pseudosingle-domain c. Multi-domain	a. Possibly biogenic	(Borradaile et al., 1993)
Carbonate/sandstones/ marine sediments	a. Irregular, needles, octahedra, and dendritic b. Elongated prismatic, bullet, hexagonal (some chains)	a. $<$10 nm to many tens of μm b. Up to ~100 nm	a. +Ti, Cr, Mn (inorganic) b. Biogenic	(Hounslow and Maher, 1996)
Chalk	a. Prismatic, bullet, cubic shapes (some chains) b. Irregular	a. Single-domain	a. Biogenic	(Montgomery et al., 1998)
Carbonate	Hollow spheres; framboids with octahedral crystals	μm-sized		(Lu et al., 1990)
Bitumen	Hollow spheres	Some single-domain/ μm-sized		(McCabe et al., 1987)
Carbonate		Single-domain	Biogenic	(McNeill and Kirschvink, 1993)
Carbonate sediments	Bullet/equidimensional	Single-domain; 50–300 nm	Biogenic	(McNeill et al., 1988)
Ancient carbonate	Spheres	15–85 μm		(Xu et al., 1994)
Limestone	a. Clusters b. Isolated grains	a. $<$1 μm b. μm-sized (single domain)	Chemical precipitates	(Suk et al., 1993b)
Oil saturated sandstones	Irregular/spheres	μm-sized		(Kilgore and Elmore, 1989)
Limestones	Spheres	15 μm common		(Elmore et al., 1987)
Deep sea sediment cores	a. Various shapes b. Angular to subhedral	a. $<$100 nm b. $<$0.1 to $>$10 μm	a. Biogenic (pure) b. + Variable Ti	(Schwartz et al., 1997)
Carbonates (1.6 Ma-2.0 Ga old)	Cuboidal, prismatic, hexagonal, bullet	Single-domain, multi-domain	Single-domain are biogenic	(Chang et al., 1989)
Ancient and present-day carbonates	Prismatic	Single-domain, multi-domain	Single-domain are biogenic	(Chang and Kirschvink, 1989, and references therein)
Carbonates	Prismatic, cubic, some chains	Single-domain	Biogenic	(Chang et al., 1987)
Precambrian stromatolites	a. Teardrop b. Spherical-oval amorphous aggregates	a. Single-domain b. 200–1000 nm	a. Probable biogenic b. Possibly biogenic	(Akai et al., 1997)
Deep sea cores/sediments	Equant (octahedral), elongated prismatic, teardrop	Single-domain	Biogenic	(Hesse, 1994)
Santa Barbara Basin	Elongated prismatic, bullet	Single-domain	Biogenic	(Stolz et al., 1986)
Deep sea sediments	Cuboidal and hexagonal	Single-domain (20–250 nm)	Biogenic	(Kirschvink and Chang, 1984)
Sediments	Cubic, bullet, elongate prisms, hexagonal; smallest are irregular	Single-domain superparamagnetic	Single domain are biogenic; superparamagnetic are inorganic	(Haese et al., 1998)
Soils			+Co, Ni, Zn, Cu, Mn, Cr, Si, and Ca	(Sidhu et al., 1980; Taylor, 1981)

(Continued)

Table A4. (Continued)

Rock type	Morphology	Size	Chemical composition/ interpretation	References
Soils	Octahedral, hexagonal, chains	10–100 nm; single-domain	Biogenic	(Fassbinder et al., 1990)
Stromatolites, marine and nonmarine	Prismatic, cuboidal, chains	Single-domain	Biogenic	(Stolz et al., 1989)
Carbonate sediments, Bahamas	Hexagonal, cubic/prismatic	Single-domain (40–100 nm)	Biogenic	(McNeill, 1990)
Lake Baikal, Siberia, sediments	Elongate hexagonal, teardrop	Single-domain	Biogenic	(Peck and King, 1996)
Queensland Plateau (carbonate platforms), Australia	Hexagonal	Single-domain (60–100 nm)	Probably Biogenic	(McNeill, 1993; McNeill et al., 1993)
Chain limestones	Framboidal/rimming	Several to tens of μm	Inorganic	(Wang and Van der Voo, 1993)
Pyroxene		Likely superparamagentic	+Al, Cr; weathering product	(Eggleton and Boland, 1982)
Sedimentary carbonates	Irregular, euhedral, aggregates, spheres	<1 (sphere) −180 μms	14 sites; inorganic; some pure and some with various elements (Ti, Cr, Ni, Mn, Zn, Si, Al, Mg, K, Ca, S, P)	(Saffer and McCabe, 1992)
Paleozoic carbonates	Spheres grains	1–70 μm; rare 50 μm	Inorganic	(Suk et al., 1992)
Glacial/interglacial	Cubic to octahedral	20–200 nm	Probably biogenic	(Lean and McCave, 1998)
Limestone	Framboids/spheres	μm		(Elmore and Crawford, 1990)
Leadville carbonates	a. Spherules	a. 5–85 μm		(Xu et al., 1998)
	b. Euhedral	b. <1 μm	b. +Ti, Mn	
	c. Fine-grain	c. 0.1–5 μm	All types inorganic	
Deep sea sediments	a. Coarse-grained; irregular; with and without ilmenite exsolution lamellae	a. Up to tens of μm	a. +Ti (inorganic)	(Vali et al., 1989)
	b. Fine-grained; some with biogenic morphology	b. Single domain	b. +Ti (inorganic); pure	
Carbonate	a. Octahedral, cubic, prismatic	a. Single-domain (mean 80 nm)	a. Biogenic (pure)	(Belkaaloul and Aissaoui, 1997)
	b. Irregular	b. 10–150 μm	b. +Ti, Ni, cr	
	c. Spheres	c. 5–30 μm		

Table A5. Magnetite in extraterrestrial samples.

Sample	Morphology	Size	Chemical composition	Mode of formation	References
CI carbonaceous chondrites	a. Rounded aggregates; crystals are equant	a. 10–30 μm; individual crystals are <1 μm	a. Trace Ni	Aqueous alteration	(Kerridge et al., 1979; Kerridge, 1970)
	b. Spherulitic; stacks of platelets	b. 5–40 μm	b. ~800 ppm Ni		
Orgueil (CI carbonaceous chondrite)	Platelets, stacking platelets, framboids	~0.5-several μm		Condensate from nebular vapor	(Jedwab, 1971)
Unequilibrated ordinary chondrites		15–20 nm			(Tople-Schadt and Muller, 1985)
CI carbonaceous chondrites	Euhedral				(Endress and Bischoff, 1966)
Type-3 ordinary chondrites	Heterogeneously distributed massive grains	Tens of μm		Hydrothermal alteration of metallic Fe	(Krot et al., 1997)
CK carbonaceous chondrites		Regions tens to hundred of μm	+Cr, Al, Ti, Ni, Mg, Mn, Si; some chemically zoned (Ni only)		(Rubin, 1993)

(Continued)

Table A5. (Continued)

Sample	Morphology	Size	Chemical composition	Mode of formation	References
C2M; Cold Bokkeveld	Euhedral/irregular/ hexagonal outlines	125 nm; narrow range			(Barber, 1981)
CI chondrites			Trace Ni	Oxidation of troilite	(Hyman and Rowe, 1983)
Interplanetary dust particles	Crystalline	50–70 nm on rims; smaller within IDPs		Heating during atmospheric entry	(Keller et al., 1992a)
Interplanetary dust particles	Irregular	<100 nm	Trace Cr	Formed by heating during atmospheric entry	(Keller et al., 1992b)
CV carbonaceous chondrite (Bali)			+Mg, Ti, Cr		(Keller et al., 1994)
CR carbonaceous chondrites	Framboidal, platelet, spherulitic			Hydrothermal alteration of elemental Fe	(Kallemeyn et al., 1994)
Shergottites	Irregular	Tens to >100 μm	+Ti		(Stolper and McSween, 1979)
Canadian sediments	Spherules	100–300 μm	+Ni	Extraterrestrial?	(Bi and Morton, 1995)
Mid-Atlantic ridge	Spherules	100–250 μm	+Mn	Extraterrestrial?	(Aumento and Mitchell, 1975)

Table A6. Synthetically and biogenic extracellularly produced magnetite.

Morphology	Size	Chemical composition[a]	Formation conditions	References
Cubic	0.05–200 μm		Aqueous, <100°C	(Schwertmann and Cornell, 1991)
Rounded, cubic or octahedral	<100 nm		Aqueous, <100°C	(Cornell and Schwertmann, 1996)
	10–1000 nm		+Carbonate 150°C	(Golden et al., 1999)
Irregular, cubic, rectangular, bullet, hexagonal plates	~10–100 nm		Heat siderite at 470°C	(Golden et al., 2000)
Generally irregular; few appear with hexagonal outline	2–171 nm		From solution; ambient T and P	(Maher, 1988)
Equidimensional and irregular	0.81–1 μm		Recrystallizing 0.5 μm magnetite crystals at 400–800°C with HI	(Heider et al., 1987)
a. Small irregular, tightly packed crystals	a. <1 μm		Reduction of hematite in aqueous solution, 350–570°C, 1–2 kbar	(Matthews, 1976)
b. Large octahedral crystals	b. >1 μm			
Equidimensional, irregular, rounded, euhedral	<1 μm to tens of μm	+Ti	High T, from Ti-containing glass	(Worm and Markert, 1987, and references therein)
a. Small euhedral	a. <100 nm	+Al	Solution, room T	(Schwertmann and Murad, 1990)
b. Larger spherical	b. 300 nm			
a. Spheres	a. 2–10 nm		Fe^{+2} and F^{+3}, pH ~ 8, room T, 1–2 days	(Jolivet et al., 1992)
b. Euhedral/prismatic/ irregular	b. 25–150 nm			
Acicular	Up to 200 nm long and 40 nm wide		Decomposition of Fe^{+3} and Fe^{+2} salts in solution with urea in a microwave; 65–100°C	(Wang et al., 1998)
Acicular rods, irregular hexagonal shapes	Mean 80 nm		Hydrothermal (130–150°C); larger crystals at higher T	(Yitai et al., 1994)
Rounded/irregular	1.5–12.5 nm		Aqueous ≤45°C	(Vayssieres et al., 1998)
			Ferrihydrite + organics heated above 300°C in air and N_2	(Campbell et al., 1997)

(Continued)

Table A6. (Continued)

Morphology	Size	Chemical composition[a]	Formation conditions	References
Equidimensional	0.2–3 μm	Pure	300°C, 2000 bars, 24 hr	(Pucher, 1969)
Octahedral, dodecahedral	Up to 100–200 μm		(a) Oxidation of Fe powder in pure water or dilute NaCl; (b) reduction of hematite with water or dilute acetic acid at NiNiO; (c) reaction of water or dilute NaCl with fine-grained magnetite or hematite at NiNiO buffer	(Cole et al., 1999)
Fibers	40–80 nm 55 nm (average)		Hematite fibers heated at 350°C in nitrogen	(Pullar et al., 1998)
a. Irregular b. Octahedral/cubo-octahedral	a. 10–60 nm b. 50–100 nm		Solution; green rust intermediary	(Mann et al., 1989)
Poorly crystalline			Fe^{+2}/Fe^{+3} ions, pH 7 $T < 353$ K	(Visalakshi et al., 1993)
Cubic	<1 μm		Fe^{+2}/Fe^{+3} ions in O_2 free aqueous system; 25–100°C, pH3–13	(Ishikawa et al., 1998)
Irregular, rounded	$\leq$20 nm		Extracellularly produced by bacteria strain GS-15	(Sparks et al., 1990; Lovley, 1991)
a. Smaller irregular b. $>$20 nm octahedral	a. Superparamagnetic b. Single-domain		Thermophillic bacteria TOR-39; 65°C produced exclusively outside of bacterial cells	(Zhang et al., 1998)

[a] Pure, unless other elements added.